AD-A035 380 TEXAS A AND M RESEARCH FOUNDATION COLLEGE STATION F/G 20/4
AN EXPERIMENTAL INVESTIGATION OF INCOMPRESSIBLE FLOW OVER DELTA--ETC(U)
DEC 76 J K NATHMAN, D J NORTON, B M RAO N00014-75-C-0255
UNCLASSIFIED ONR-CR215-231-3 NL

1 OF 1
AD-A
035 380

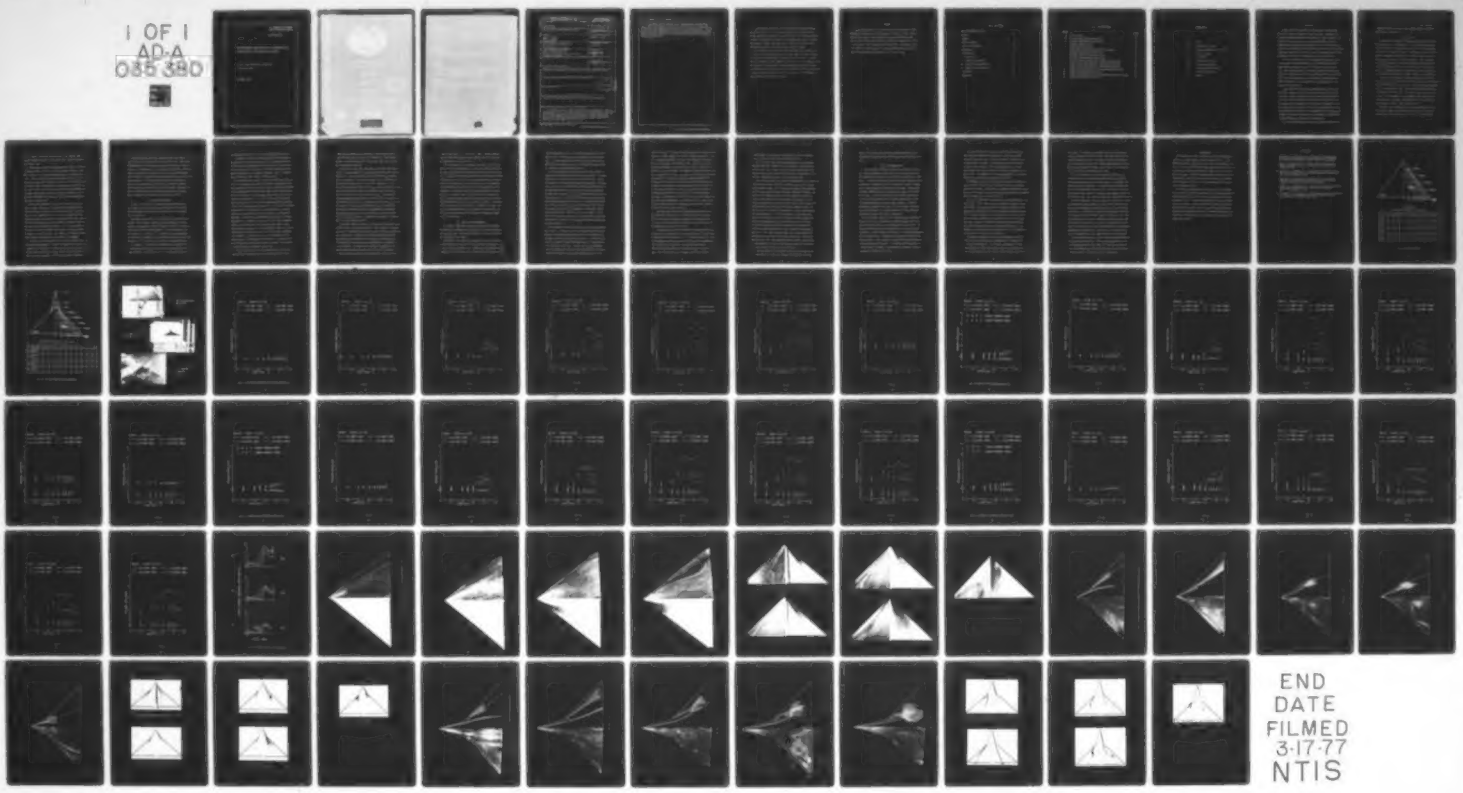

END
DATE
FILMED
3-17-77
NTIS

AN EXPERIMENTAL INVESTIGATION OF INCOMPRESSIBLE FLOW OVER DELTA AND DOUBLE-DELTA WINGS

TEXAS A AND M RESEARCH FOUNDATION
COLLEGE STATION

DECEMBER 1976

REPORT DOCUMENTATION PAGE

READ INSTRUCTIONS BEFORE COMPLETING FORM

1. REPORT NUMBER	2. GOVT ACCESSION NO. / 3. RECIPIENT'S CATALOG NUMBER
4. TITLE (and Subtitle): An Experimental Investigation of Incompressible Flow Over Delta and Double-Delta Wings	5. TYPE OF REPORT & PERIOD COVERED: Jan. 1975 - Dec. 1976 Technical Report
	6. PERFORMING ORG. REPORT NUMBER
7. AUTHOR(s): James K. Nathman, David J. Norton, Balusu M. Rao	8. CONTRACT OR GRANT NUMBER(s): N00014-75-C-0255
9. PERFORMING ORGANIZATION NAME AND ADDRESS: Texas A&M Research Foundation, F. E. Box H, College Station, TX 77843	10. PROGRAM ELEMENT, PROJECT, TASK AREA & WORK UNIT NUMBERS: NR 215-231
11. CONTROLLING OFFICE NAME AND ADDRESS: Office of Naval Research, Vehicle and Propulsion Programs, Code 211, Arlington, VA 22217	12. REPORT DATE: December 1976 / 13. NUMBER OF PAGES: 78
14. MONITORING AGENCY NAME & ADDRESS (if different from Controlling Office)	15. SECURITY CLASS. (of this report): Unclassified / 15a. DECLASSIFICATION/DOWNGRADING SCHEDULE

16. DISTRIBUTION STATEMENT (of this Report)

Approved for public release; distribution unlimited. Reproduction in whole or in part is permitted for any purpose of the United States Government

17. DISTRIBUTION STATEMENT (of the abstract entered in Block 20, if different from Report)

18. SUPPLEMENTARY NOTES

19. KEY WORDS (Continue on reverse side if necessary and identify by block number)

Vortex Flow; Leading Edge Separation; Delta Wings; Double-Delta Wings

20. ABSTRACT (Continue on reverse side if necessary and identify by block number)

An experimental study of the flow over delta and double-delta wings was conducted in a 7' x 10' low speed wing tunnel. The configurations tested were AR-3 and AR-4 delta wings and the AR-4 wing which was modified with AR-1 and AR-2 strakes attached to form double-delta wings. Pressure measurements, surface flow visualization, and vortex core visualization studies were conducted over a wide range of angles of attack.

DD FORM 1 JAN 73 1473 EDITION OF 1 NOV 65 IS OBSOLETE

At low angle of attack the AR-3 wing displayed a well defined vortex core with a vortex burst present over the wing. Above 15° angle of attack the vortex core was replaced by a turbulent core of vorticity. The AR-4 wing did not generate a well defined vortex core even at low angles of attack. The addition of a highly swept strake to the apex of AR-4 wing introduces a secondary vortex core which stabilizes the rollup of vorticity on the main wing, thus delaying the onset of stall. The delay in stall increases as the sweep angle of the strake increases.

ABSTRACT

An experimental study of the flow over delta and double-delta wings was conducted in a 7' x 10' low speed wind tunnel. The configurations tested were AR-3 and AR-4 delta wings and the AR-4 wing which was modified with AR-1 and AR-2 strakes attached to form double-delta wings. Pressure measurements, surface flow visualization, and vortex core visualization studies were conducted over a wide range of angles of attakc.

At low angles of attack the AR-3 wing displayed a well defined vortex core with a vortex burst present over the wing. Above 15° angle of attack the vortex core was replaced by a turbulent core of vorticity. The AR-4 wing did not generate a well defined vortex core even at low angles of attack. The addition of a highly swept strake to the apex of AR-4 wing introduces a secondary vortex core which stabilizes the rollup of vorticity on the main wing, thus delaying the onset of stall. The delay in stall increases as the sweep angle of the strake increases.

FOREWORD

The work described in this technical report was performed by Texas A&M Research Foundation for the Department of the Navy, Office of Naval Research, Arlington, Virginia under contract number N00014-75-C-0255. The Scientific Officer who initiated this research program was Mr. Thomas L. Wilson and he was followed by CDR William Albers. The present Scientific Officer of the program is Dr. Robert Whitehead and the Director of the Vehicles and Propulsion Programs is Mr. David S. Siegel.

TABLE OF CONTENTS

LIST OF ILLUSTRATIONS

NOMENCLATURE

b	- span
AR	- aspect ratio = $2b/C_R$
C_p	- pressure coefficient = $(P-P_\infty)/\frac{1}{2}\rho V_\infty^2$
α	- angle of attack
c_R	- root chord
c_{Ro}	- reference root chord
P	- local static pressure
P_∞	- free stream static pressure
V_∞	- free stream velocity
ρ	- density

INTRODUCTION

Under contract to the Office of Naval Research, Texas A&M University is conducting experimental and theoretical investigations leading to the explorations of the vortex flow over wings with flow separation at the leading edge. Leading-edge separation often accompanies the flight of high-performance aircraft at high angles of attack as a consequence of the thin airfoil sections and severe leading-edge sweep required for supersonic flight. Advantageous use of this phenomenon will increase the maneuverability of these aircraft.

Early in the program thin, sharp-edged delta wings were chosen as the subject of the investigation. Besides exhibiting leading-edge separation even at low angles of attack, delta wings have a very simple planform which has led to many attempts at theoretical analysis. Together with the store of experimental data gathered here and in previous investigations, this theoretical simplicity makes delta wings appear to be the keystone in the development of a unified vortex flow theory.

Some of the first experiments centered around an aspect ratio two wing. Extensive tests into the steady and unsteady flow about this wing provided the requisite skill to investigate the higher aspect ratio wings of more practical interest. At the same time, it was recognized that unsteady flow tests could be suspended in order to concentrate on a planform typical of a high-performance aircraft. Consideration of the value of the experimental work in advancing the theoretical research led to the choice of modeling an advanced Naval aircraft planform as a double-delta configuration.

The test program covered by this study specified continuing the

research into delta wings at aspect ratios of 3 and 4 simulating an advanced planform by fitting a highly swept strake to the apex of the aspect ratio 4 delta wing.

I. TEST SET-UP

The models used in these studies were two delta wings with overall aspect ratios of three and four. The wings had a common span of 1.22m (4 ft) with root chords of 0.81m (2.67 ft) for the AR3 model and).61m (2 ft) for the AR4 model. The aspect ratio four wing incorporated a detachable apex forward of 18.75% root chord which could be replaced with either of two apex extensions. These extensions had leading-edge sweeps corresponding to aspect ratios of one and two, and lengths of 0.46m (18 in) and 0.23m (9 in) respectively. The span of the extensions equaled the span of the wing at the juncture, so that the wing with extension formed a double delta configuration.

A total of four configurations were tested, as illustrated in Figs. 1a and 1b. These are designated by the aspect ratio of the wing (AR3, AR4) and of the apex (A1, A2, A3, A4). The last two apex designations refer to ordinary delta wings. The AR4-A2 configuration had an overall aspect ratio of 3.86 while the AR4-A1 configuration had a ratio of 3.62. All the models were constructed of 9.5mm (.375 in) thick aluminum plate. The leading edges were beveled at 20° along the lower surface to insure a sharp separation line.

The tests were conducted in the Texas A&M University 7x10 foot wind tunnel, using a sting mount system (Figures 2 and 3) with a useable angle-of-attack range of -8° to 26°. The sting support

incorporated a Trans-Tek Series 600 angular displacement transducer which provided an angle-of-attack signal for a digital voltmeter in the control room.

The pressure distribution measurements were taken at 2.5 degree increments from -7.5° to 25° at a nominal dynamic pressure of 480 N/m^2 (10 psf). The resulting Reynolds number of the AR4 wing was 1.1 x 10^6. Both wings were designed with 40 upper surface ports, the positions of which are illustrated in Figure 1. In addition, the AR4 wing had 32 lower surface ports which corresponded in position with the upper surface ports (excluding those over the leading-edge bevel). At model installation time, two of the upper surface ports on the AR4 wing were found to be unuseable. No pressure measurements were made over the extensions.

Brass tubing imbedded in the wing led from each port to the trailing edge, Figure 4, where flexible tubing completed the connection with two scanivalves in the rear of the sting. Each valve successively connected the ports to its own Validyne DP9 pressure transducer which was referenced to a reference tunnel static pressure. The transducer analog signal was converted to a digital signal and sampled by a Data General NOVA computer. An oscillograph trace of the transducer signal indicated the maximum fill time was 30 msec. Therefore, a delay of 100 msec. was included in the sampling program. Each data point was computed as an average of five samples.

The upper surface flow patterns over the four configurations were observed and photographed at 5 degree increments from 5 to 25 degrees. A suspension of lampblack in kerosene was painted over the white-colored wings and the tunnel quickly run up to the same speed as that of the pressure measurements. The resulting pattern indicated the

direction and relative speed of the surface flow.

Flow visualization techniques were also used to observe the external flow over the wings, especially the vortex cores. Both liquid Nitrogen/steam and oil smoke were injected into the flow to mark the vortex core. Photographs of the injectant were obtained by introducing smoke at the apex (to visualize the apex vortex) and, for the wing with extension, at the juncture between extension and wing (to visualize the wing vortex). Both planform and profile photos were made to permit a three-dimensional determination of the vortex core paths. Movie footage was also taken to record the continually changing vortex structure over the AR4 wing and AR4-A1 double delta as the models were pitched from zero to maximum useable angle of attack.

II. PRESSURE DISTRIBUTION

Figure 5 and 6 present the measured pressure coefficients for the aspect ratio 3 and 4 delta wings while Figure 7 and 8 are the pressure distributions of the aspect ratio 4 wing with the A2 and A1 apex extensions.

The lower surface bevel, while introducing a slight camber into the wing, did not appear to affect the results greatly. The bevel produced an asymmetry with respect to angle of attack in the pressure distribution of all four configurations. This can be noted by comparing the a ($\alpha = -5°$) and c ($\alpha = 5°$) graphs of each configuration. As can be seen in Figure 5a, no suction peaks are present on the lower surface at $\alpha = -5°$, while they are present on the upper surface at $\alpha = 5°$, Figure 5c. The pressure distributions also indicate no vortex separation over the upper surface for any configuration at zero angle of attack. Distributions at $\alpha = 2.5°$ do indicate that leading

edge separation occurs for this and every configuration above 2.5°.

In general, the form of the spanwise pressure distribution over the upper surface of the delta wings is a flat inboard valley with a suction peak at approximately the 70% local span. As the angle of attack increases, the form remains relatively unchanged while the magnitude increases, as indicated in Figure 9a. There is some movement of the suction peak inboard at higher angles.

One exception to this rule is the result of bursting of the vortex core. As observed by Lambourne and Bryer[1], the presence of the burst upstream of a chord station will lead to a pressure distribution at that station which "is much flatter than would be expected in the absence of the burst." For the aspect ratio 3 wing, the core bursts near the trailing edge at α = 10°. By 15° the burst has moved to the 40% chord station. A look at the spanwise pressure distributions at the 20, 40, and 60% chord stations for α = 10, 15, and 20° (Figure 9) shows that for a station upstream of the burst (20% c_R), the only change in the distribution with angle of attack is an increase in magnitude. The station just downstream (40% c_R) shows an increase in magnitude when α increases from 10° to 15°; but at 20° the maximum suction is less than that at 15° while the suction peak is much broader than the peak at 15°. Further downstream (60% c_R), a sharply rising suction peak occurs only at α = 10° after which the maximum suction drops as α increases to 15°. The suction peak at 15° is broader than at 10° and continues to broaden as α increases to 20°, while the maximum suction remains almost unchanged. These patterns correlate well with the movement of the burst.

It was originally hoped to track the position of the burst by the distortion it produced in the pressure distribution. This pro-

cedure was confounded by the uncertainty of the distance from the burst to the affected chord station and the difference in core structure between the present wings and the lower aspect ratio wings for which the procedure was successful.

The addition of the apex extensions to the aspect ratio 4 wings results in radical changes to the pressure distribution over the wing. Foremost is the drop in suction at the station (20% c_{Ro}) directly aft of the extension. The lower the aspect ratio of the extension is the lower the maximum suction. With the A2 extension at $\alpha = 10°$ (Figure 7d) the maximum suction at 20% c_{Ro} is the same as that at 40% c_{Ro}. With the A1 extension (Figure 8d) the maximum suction at 40% c_{Ro} is about a factor 2.5 times the suction at 20% c_{Ro}. This reversal in trend compared to the delta wing is not solely due to the loss of suction at 20% c_{Ro} but also to the increased suction at 40% c_{Ro}. In fact, the stations further downstream (60 and 80% c_{Ro}) also show marked increases in suction when the wing is equipped with an extension. Considering the larger span of the aft stations, and the increased area of the apex, the result is probably the increased lift at higher angles of attack noted by Wentz.[3]

The second significant change in the pressure distribution caused by the addition of the apex extensions is the induction at low angles of attack of a secondary suction peak inboard of the main suction peak. This is best seen in Figure 8d at the 40% reference chord station. These secondary suction peaks occur at angles of attack between 0 and 5 degrees for the A2 extension and between 0 and 15 degrees for the A1 extension. Two suction peaks indicate the presence of two separate vortices above the wing; one resulting from the rollup of the vorticity shed by the apex extension and the other by a distinct

rollup of the vorticity shed by the main wing. Beyond the maximum angle at which the secondary peak is observed the two vortices are so intertwined as to act like one.

The third effect of the low aspect ratio apex, which is apparent in the pressure measurements, is the delay in the onset of stall. The upper surface pressure distributions for the aspect ratio 3 wing at 25° (Figure 5g) and the aspect ratio 4 wing at 20° and 25° (Figures 6f and 6g) are flat. There are no well-defined vortex effects characteristic of delta wings at lower angles of attack. Measurements at intermediate angles narrow the stall point to between 22.5 and 25 degrees for the aspect ratio three wing and between 17.5 and 20 degrees for the aspect ratio 4 wing. Despite their higher aspect ratio, the double delta wings continue to show vortex suction peaks at 25° where the aspect ratio 3 delta wing has stalled. The behavior of the AR4-A2 pressure distribution as it flattens out from α = 22.5° to α = 25° indicates that the wing is probably close to stall; but the steadily increasing peaks of the AR4-A1 configuration suggest it is well below stall.

III. SURFACE FLOW OBSERVATIONS

In order to understnad the mechanisms producing the pressure distributions, a complementary study of the surface flow patterns on the wings was made. The technique employed is discussed in the test set-up section of this report.

Peckham[4] has noted that for delta wings the dip in the spanwise pressure distribution inboard of the suction peak corresponds to the position of the reattachment line. Comparison of the present pressure measurements with the upper surface flow patterns on the delta wings,

illustrated Figures 10 and 11, show this observation to be correct. When the lines of maximum suction are graphed over the surface patterns it is also seen that the peak occurs at the same span-wise position as the inflection point of the surface flow pattern, that is, the point of maximum spanwise velocity.

The flow patterns correlate well with the onset of stall. In Figure 10d, the pattern on the aspect ratio 3 wing at $\alpha = 25°$ shows that the flow is well attached over about half the wing. The reattachment line has moved to the centerline of the wing. The white area near the tip is the position of a whorl pattern where the kerosene/lampblack was seen to move along the leading edge towards the apex, flow inboard and aft to the trailing edge than out to the leading edge, etc. This pattern corresponds to the flat pressure distribution recorded at 25°, Figure 5g. An identical description can be given for the flow pattern over the aspect ratio 4 wing at 20° (Figure 11d) which also corresponds to a flat upper surface pressure distribution. Above the initial stall angle ($\alpha = 25°$, Figure 11e) the entire upper surface is a large whorl pattern with the flow moving from the wing tip toward the apex and curling back along the centerline.

Just outboard of the maximum suction line (on surface patterns below stall), is a white streak. Often inboard of this streak is a dark line of lampblack deposit which signifies the presence of a secondary separation and vanishing shear stress. The white streak itself is a region of high surface shear since all the surface particles have been cleared off. Probably this region represents a region of predominately chordwise flow concentrated by the tangential surface flow induced by primary and secondary vortices. At low

angles of attack as in Figure 10a the separation line is quite straight. However, at higher angles this line kinks outboard as shown in Figure 10b. Lambourne and Bryer[1] associate this bending with the outward spread of turbulence from the vortex burst. Wentz[5], too, relates the outward movement of the separation line with an increase in effective vortex core diameter. This method of determining the position of the vortex burst is suspect according to evidence given by Earnshaw and Lawford[6]. They make the distinction between movement of the separation line due to vortex bursting and that associated with the transition from laminar to turbulent separation of the surface flow. If turbulent separation is the cause, the separation line will be displaced outwardly along the span, while if vortex breakdown is the cause, the separation line will still be along a ray from the apex but with decreased sweepback. In the present case it seems possible that the transition occurs simultaneously with the burst, obscuring the position of the vortex core burst.

While some correlation exists for both methods of determining the position of the burst over the aspect ratio 3 wing, the suitability of either one becomes a moot point for the aspect 4 wing in light of the failure during the present tests to observe a tight core structure or burst over that wing.

The presence of two separate vortices above the wings with apex extensions as was surmised by the two pressure peaks, is most clearly indicated by the flow patterns at $\alpha = 5°$, Figures 12a and 14a. While the secondary pressure peak caused by the apex vortex was detectable only to about half of the chord, the surface pattern shows a continuous secondary separation line from the apex to the trailing edge. This indicates that the secondary suction line extends to the

trailing edge. The wing vortex also produces a distinct separation line and region of high induced Tangential velocity.

At 10°, (Figure 12b) the AR4-A2 configuration had no secondary pressure peaks; and, indeed, the surface pattern is consistent with the conclusion that the apex and wing vortices intertwine quickly to form one vortex. At all angles above 10°, the surface pattern is very similar in appearance to that of an ordinary delta wing.

The surface patterns of the AR4-A1 configuration at 10° (Figure 14b) indicate that there are still two separate vortices that lie above the two pressure peaks. At 15° the secondary pressure peak disappears aft of 40% c_{Ro} and the maximum peak moves substantially inboard. The kinking of the separation line on the wing indicates that the vortices have interacted strongly and features of the pattern can no longer be attributed to a distinct second vortex. At 20° (Figure 14d) the separation and maximum suction lines are violently kinked. In fact, while the suction line was graphed as a single line through the four chord stations, it may be discontinuous. A possible explanation for the pattern is that the two vortices form a double helix which alternately places one of the vortices close to the wing. At 25°, the pressure distribution and surface flow pattern both indicate the apex and wing vortices have intertwined to function as one vortex. The single secondary separation line and orderly surface pattern is very similar to the AR4 delta wing at 10° or the AR4-A2 wing at 15° or 20° suggesting that the greater the difference in sweep between the strake and the wing the higher will be the angle of attack at which the two vortices intertwine.

The flow patterns for the double delta wings also confirm the fact that they have significantly higher stalling angles than the

aspect ratio 4 delta wing; and higher even than the aspect ratio 3 delta wing, although the double delta wings have aspect ratios greater than 3.

V. VORTEX FLOW VISUALIZATION

It was originally intended to observe the position of the vortex burst and the trajectory of the vortex core over the aspect ratio 3 and 4 delta wings to supplement the study of the aspect ratio 2 delta wing. In that earlier study the vortex core, when seeded with smoke, appeared as a concentrated filament of smoke with the burst showing up as a sharp expansion and diffusion of the smoke. Unfortunately, no sharply defined core was observed over the aspect ratio 3 and 4 delta wings. It was first thought that the seeding technique was at fault, but upon returning to the original aspect ratio 2 wing the concentrated core structure was again observed. Schlieren observations by Wentz[2] confirm that it is not the fault of the visualization technique. This indefiniteness of structure has made a quantitative study of the vortices impractical.

Up to an angle of attack of 10° (Figure 10a) the core above the aspect ratio 3 wing is too weak to be properly seeded; and it does not entrain enough smoke to resolve the position of the burst. The most well-defined core above the aspect ratio 3 wing occurs at 15° (Figure 10b). Here it appears that a burst is visible at approximately 35% of the root chord. At higher angles of attack (Figures 10c and 10d), the vortices are visualized as large cones of smoke with a non-defined core even near the apex. The vortices above the aspect ratio 4 delta wing at all angles of attack below stall appear as cones when injected with smoke (Figures 11a-d).

In comparing the vortex structure over the delta wings at the point where the pressure distribution has a flat, stall pattern (Figures 10d and 11d) to the structure at previous angles of attack, no marked change is evident. Only after the pressure distribution is very flat and the wing surface pattern develops into a large whorl (Figure 11e) does the external flow indicate a breakdown in the vortex flow. This breakdown is quite complete though, as illustrated by the lack of structure of the smoke in Figure 11e.

Photographs of the vortex structure above the double delta wings (Figures 13 and 15) confirm the conclusions drawn from the pressure and surface flow data. These figures are composite photographs showing the apex vortex on the right while the right hand wing vortex photograph has been reversed and is shown on the left.

At 5°, the AR4-A2 configuration shows two independent vortex cores (Figure 13a). By 10°, these two cores intertwine just past the apex-wing juncture. The occurrence of this interaction between 5 and 10° compares well with Wentz's[3] data for an AR2.1 wing with an A1 strake. At 15°, the apex vortex bursts as it interacts with the wing vortex. The burst moves upstream to the wing juncture at 20°. At 25°, the wing vortex indicates a breakdown of the vortex formation over the wing, while the apex vortex bursts before the wing juncture. The movement of the apex vortex burst suggests that it is the interaction with the wing vortex which triggers the burst.

The AR4-A1 configuration also has two independent vortices at 5° (Figure 15a) but these remain independent at 10° (Figure 15b). This figure illustrates the long filament appearance of a vortex core produced by a highly swept leading edge, in counterpoint to the cone of smoke representing the vortices over the aspect ratio 3 and 4

delta wings. Of interest are the photos which show that the wing vortex on the AR4-A1 configuration has a more well-defined core than on the ordinary delta wing. The change in vorticity shedding rate or the reduction of the effective leading-edge sweep due to the spanwise velocity induced by the apex vortex results in a core structure similar to that over lower aspect ratio wings.

At 15° (Figure 15c), the wing vortex bursts near 60% c_{Ro}. The apex vortex bends outboard and passes under the wing vortex. Profile photographs show that the apex vortex is very straight from the apex to the wing juncture. Its trajectory above the wing then levels off and bends down toward the wing. At the point where the two vortices cross, the core of the apex vortex appears to be in contact with the wing, while the wing vortex has lifted well off the wing.

At 20° (Figure 15d), the apex vortex has lifted further off the wing and bursts slightly ahead of the wing vortex. Near its burst, the apex vortex bends down toward the wing as it curves around the wing vortex. The trajectory of the wing vortex changes very little as the angle of attack increases further. Finally at 25°, the wing vortex can be seen to rise very rapidly from the wing, burst, and curve back down to the wing. This rapid rise leaves only the apex vortex in close proximity to the wing, and hence the surface pattern's appearance of being made by a single vortex. The bursting of the wing is accompanied by a very sudden bursting of the apex vortex.

The complex rollup of the vortices above the double delta wings may be subject to hysteresis. While the flow appeared to be very stable when perturbed by smoke probes, all the data for the double delta configurations was obtained as the angle of attack increased, so the possibility of hysteresis cannot be discounted.

CONCLUSIONS

At low angles of attack, the aspect ratio 3 wing displayed characteristics of lower aspect ratio delta wings, that is, a well-defined vortex core with vortex burst present over the wing. Above $\alpha = 15°$, this structure was lost, being replaced by a turbulent core of vorticity which was present over the aspect ratio 4 wing at all angles of attack. Although wing pressure measurements and surface flow patterns do not reveal any marked effect due to the change in vortex structure, the loss in fine structure appears to be a preliminary indication of stall.

By adding a highly swept strake to the apex of a high aspect ratio delta wing, a well-defined vortex core can be introduced which stabilized the rollup of vorticity from the main wing and delayed the onset of stall. Although the double delta wing has an aspect ratio less than that of the original wing, the double delta wings performed better at high angles of attack than would an ordinary delta wing of the same aspect ratio. The experiments further indicates that the stall angle was increased as the sweep angle of the strake was increased.

REFERENCES

1. Lambourne, N.C. and Bryer, D.W., "The Bursting of Leading-Edge Vortices - Some Observations and Discussions of the Phenomenon," British Aeronautical Research Council, R&M 3283, London 1962.

2. Wentz, W.H. and Kohlman, D.L., "Wind Tunnel Investigations of Vortex Breakdown on Slender Sharp-Edged Wings," NASA CR-98737, Washington, 1968.

3. Wentz, W.H. and McMahon, M.C., "An Experimental Investigation of the Flow Fields about Delta and Double-Delta Wings at Low Speeds," NASA CR-521, Washington, 1966.

4. Peckham, D.H., "Low-Speed Wind Tunnel Tests on a Series of Uncambered Slender Pointed Wings with Sharp Edges," British Aeronautical Research Council, R&M 3186, London, 1961.

5. Wentz, W.H. and McMachon, M.C., "Further Experimental Investigations of Delta and Double-Delta Wing Flow Fields at Low Speeds," NASA CR-714, Washington, 1967.

6. Earnshaw, P.B. and Lawford, V.A., "Low-Speed Wing Tunnel Experiments on a Series of Sharp-edged Delta Wings," British Aeronautical Research Council, R&M 3424, London, 1964.

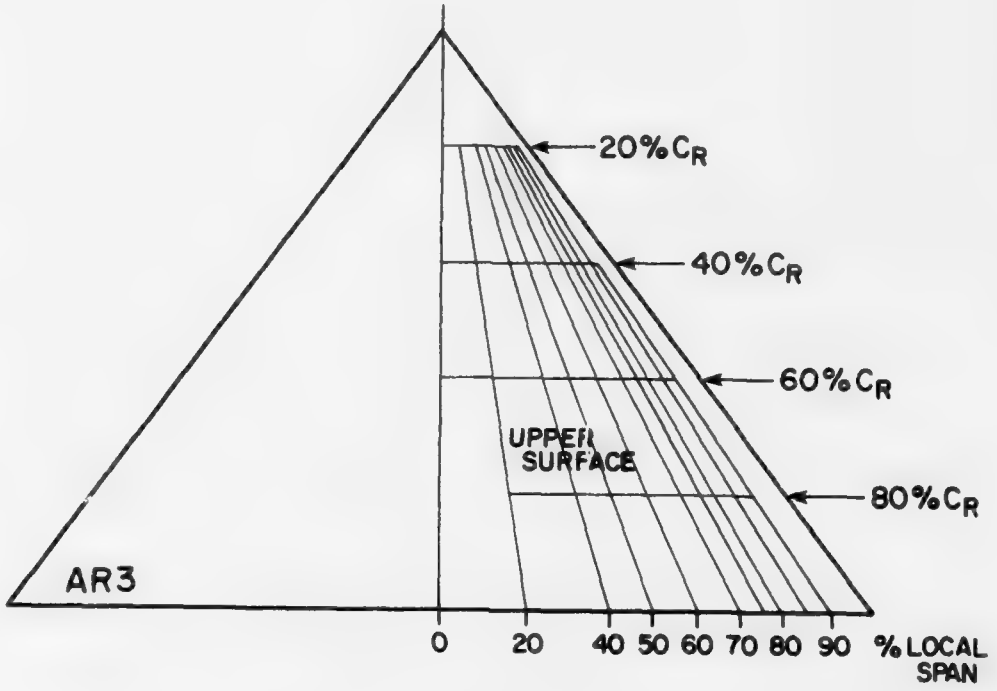

UPPER SURFACE

Pressure Port Locations - % Local Span

C_L	0	20	40	50	60	65	70	75	80	85	90
20%	.	.	.	.	.	.	.	.	.	.	
40%	.	.	.	.	.		.	.	.	.	.
60%	.	.	.	.	.		.	.	.	.	.
80%		.	.	.	.		.	.	.	.	.

FIG. 1a AR4 TEST MODEL

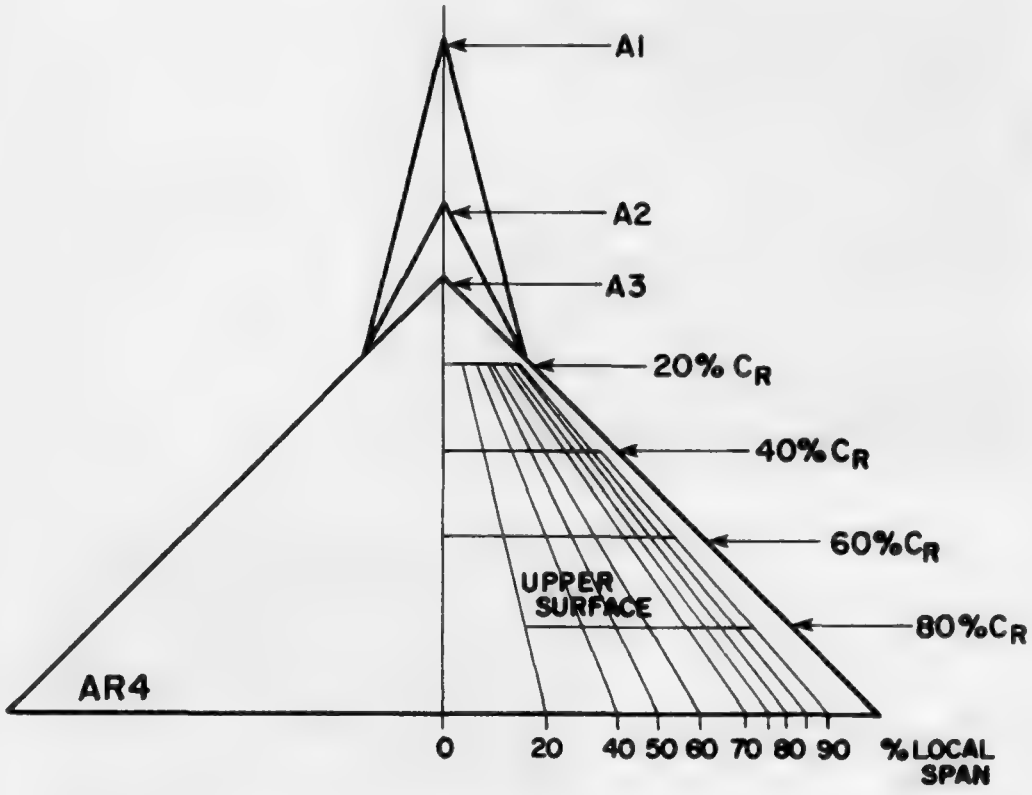

Pressure Port Locations - % Local Span

C_R	Surface	0	20	40	50	60	65	70	75	80	85	90
20%	upper	.	.	.	.	.	.	.	.	.	.	
	lower	.	.	.	.	.	.					
40%	upper	.	.	.	.	.		.	.	.	.	.
	lower	.	.	.	.	.		.	.	.		
60%	upper	.	.	.	.	.		.	.	.	.	.
	lower	.	.	.	.	.		.	.	.	.	
80%	upper		.	.	.	.		.	.	.	.	.
	lower		.	.	.	.		.	.	.	.	.

FIG. 1b AR3 TEST MODEL WITH APEX EXTENSIONS

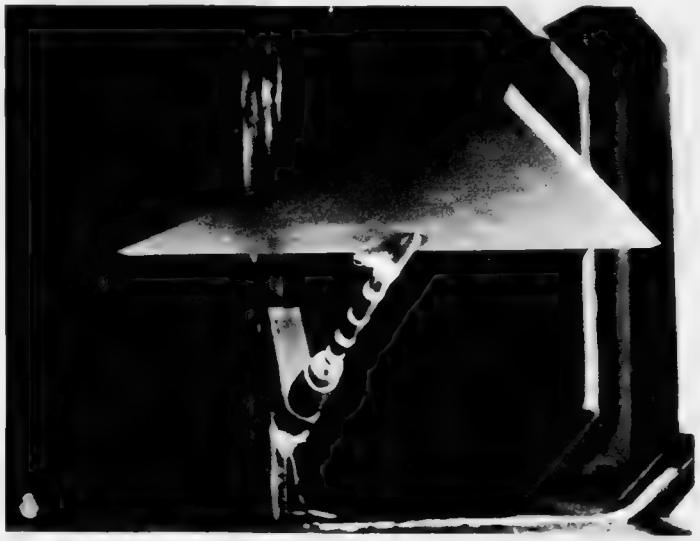

FIG. 2 PRESSURE MEASUREMENTS OVER AR3 WING

FIG. 3 SURFACE FLOW AR4-A1 WING

FIG. 4 TRAILING EDGE OF AR3 WING

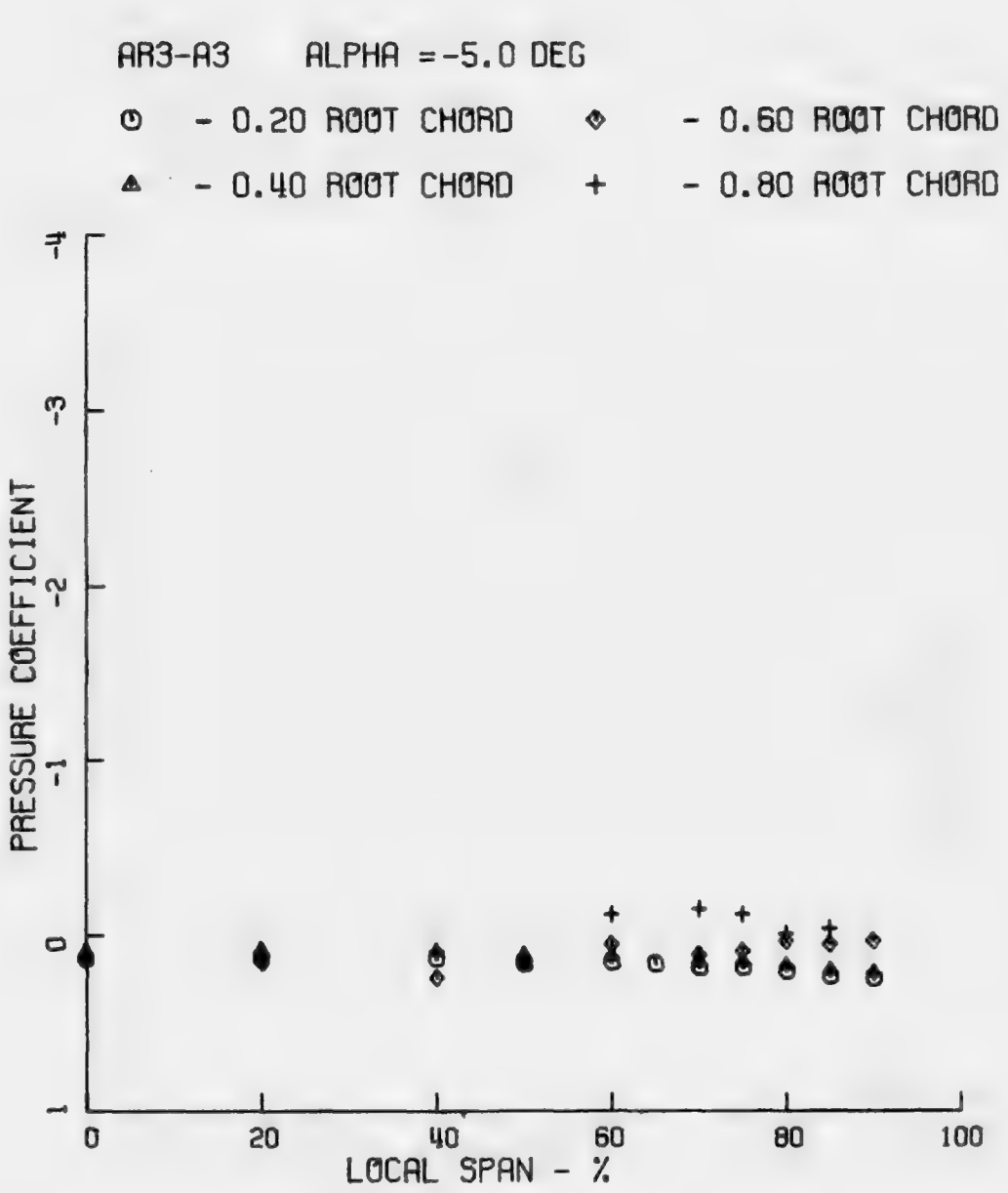

FIG. 5a UPPER SURFACE PRESSURE DISTRIBUTION OVER AR3 WING

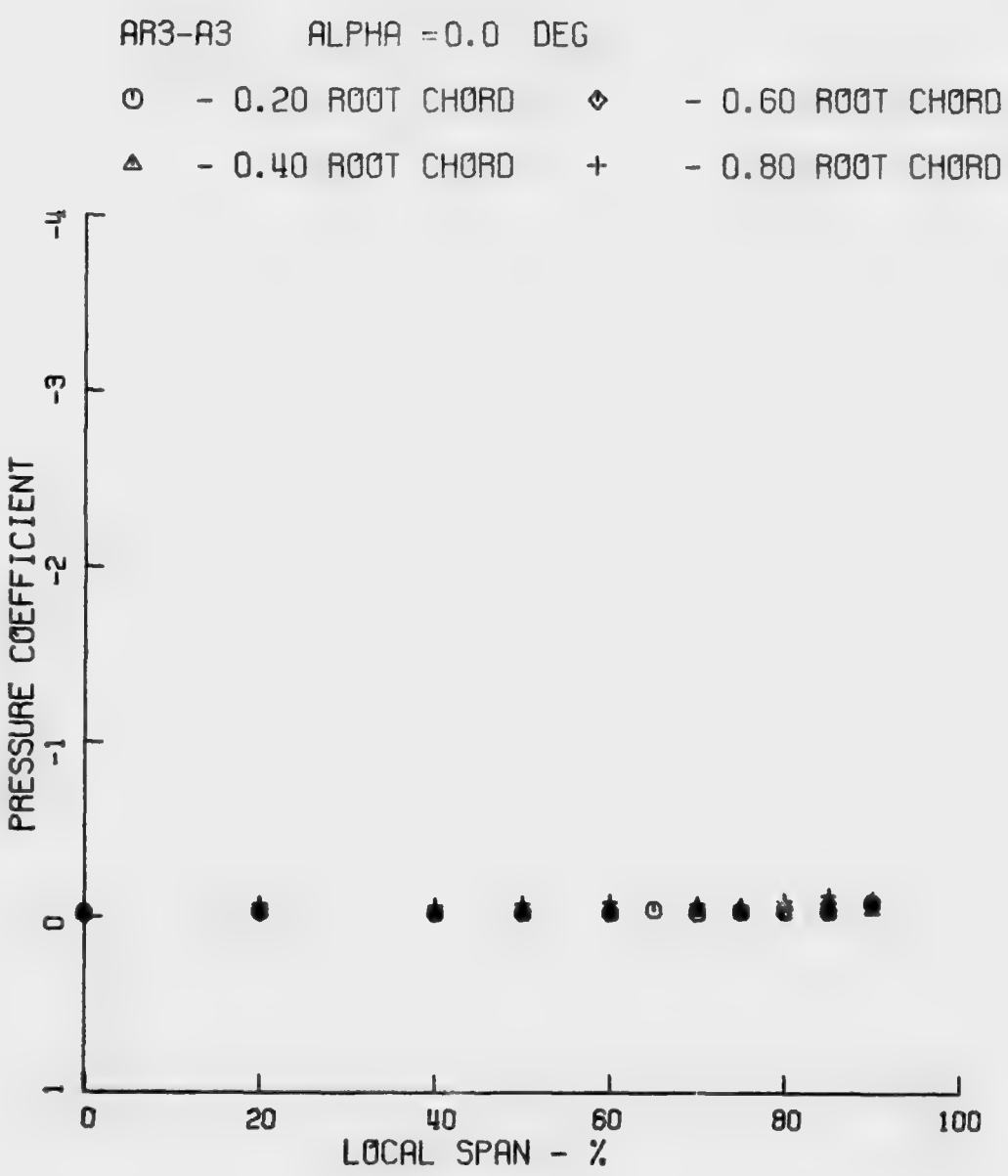
AR3-A3 ALPHA =0.0 DEG
- 0.20 ROOT CHORD
- 0.40 ROOT CHORD
- 0.60 ROOT CHORD
- 0.80 ROOT CHORD
PRESSURE COEFFICIENT
-4
-3
-2
-1
0
1
0
20
40
60
80
100
LOCAL SPAN - %

FIG. 5b

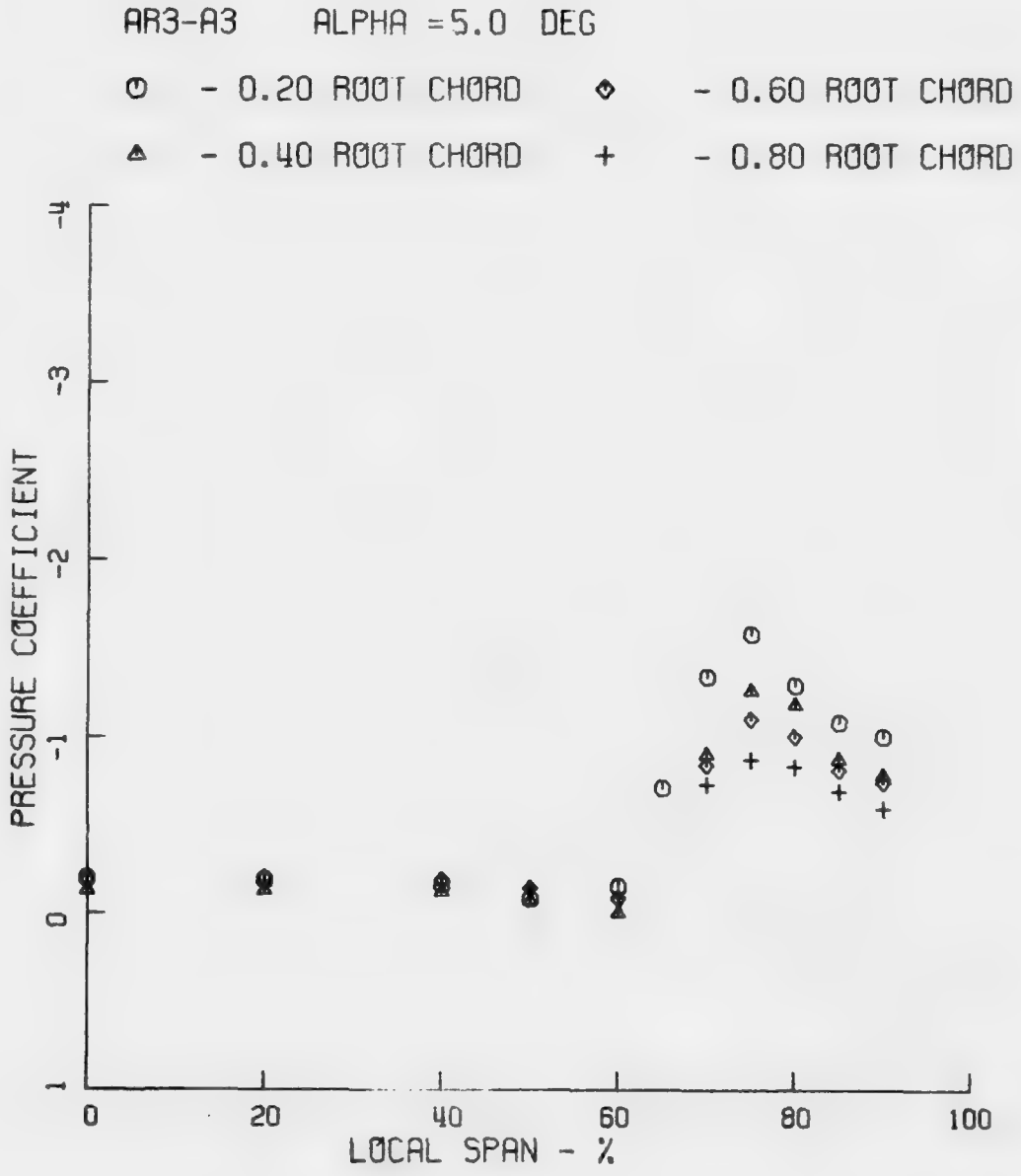
AR3-A3 ALPHA =5.0 DEG
- 0.20 ROOT CHORD
- 0.40 ROOT CHORD
- 0.60 ROOT CHORD
- 0.80 ROOT CHORD
PRESSURE COEFFICIENT
-4
-3
-2
-1
0
1
0
20
40
60
80
100
LOCAL SPAN - %

FIG. 5c

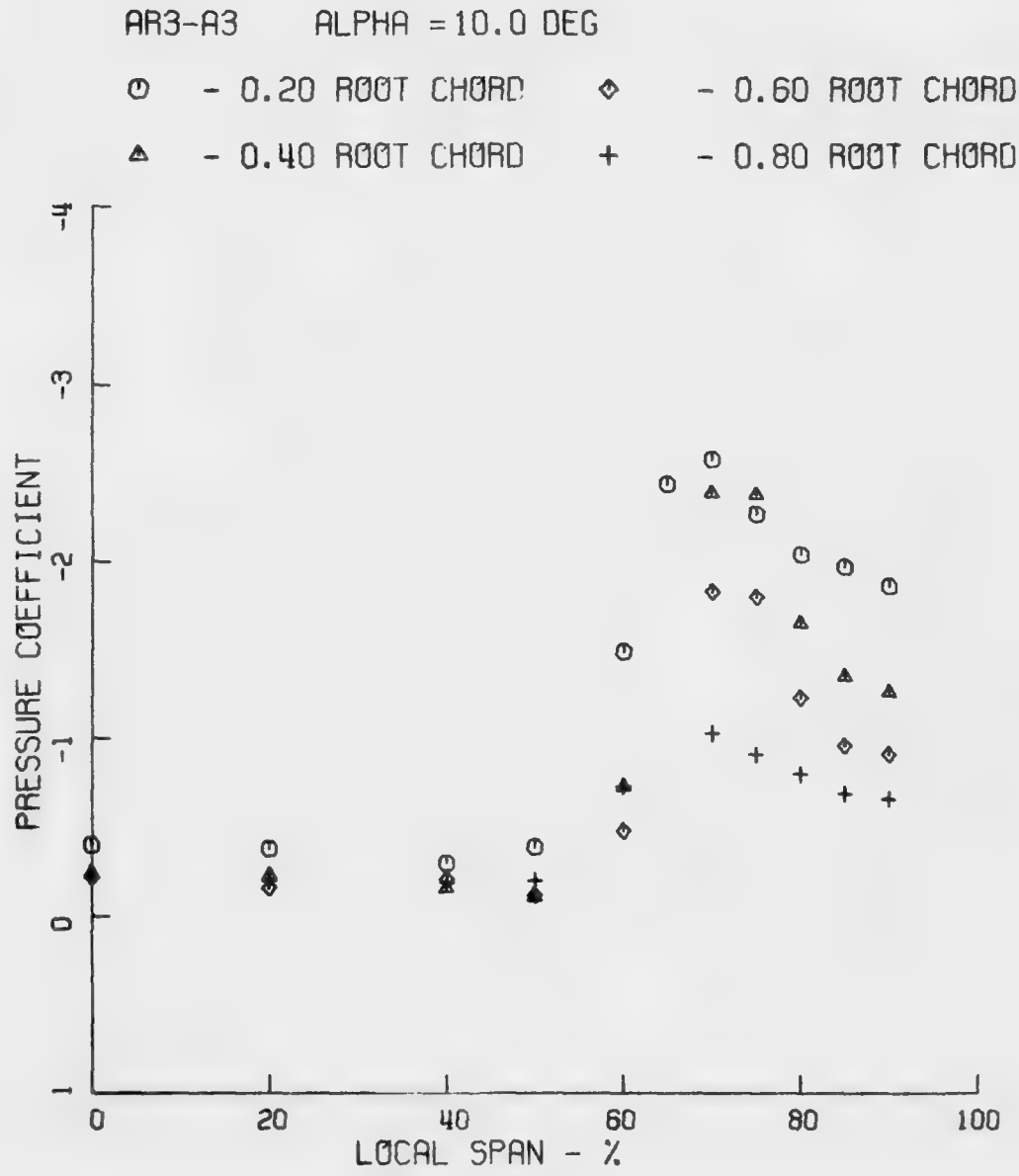
AR3-A3 ALPHA = 10.0 DEG
- 0.20 ROOT CHORD
- 0.40 ROOT CHORD
- 0.60 ROOT CHORD
- 0.80 ROOT CHORD
PRESSURE COEFFICIENT
-4
-3
-2
-1
0
1
0
20
40
60
80
100
LOCAL SPAN - %

FIG. 5d

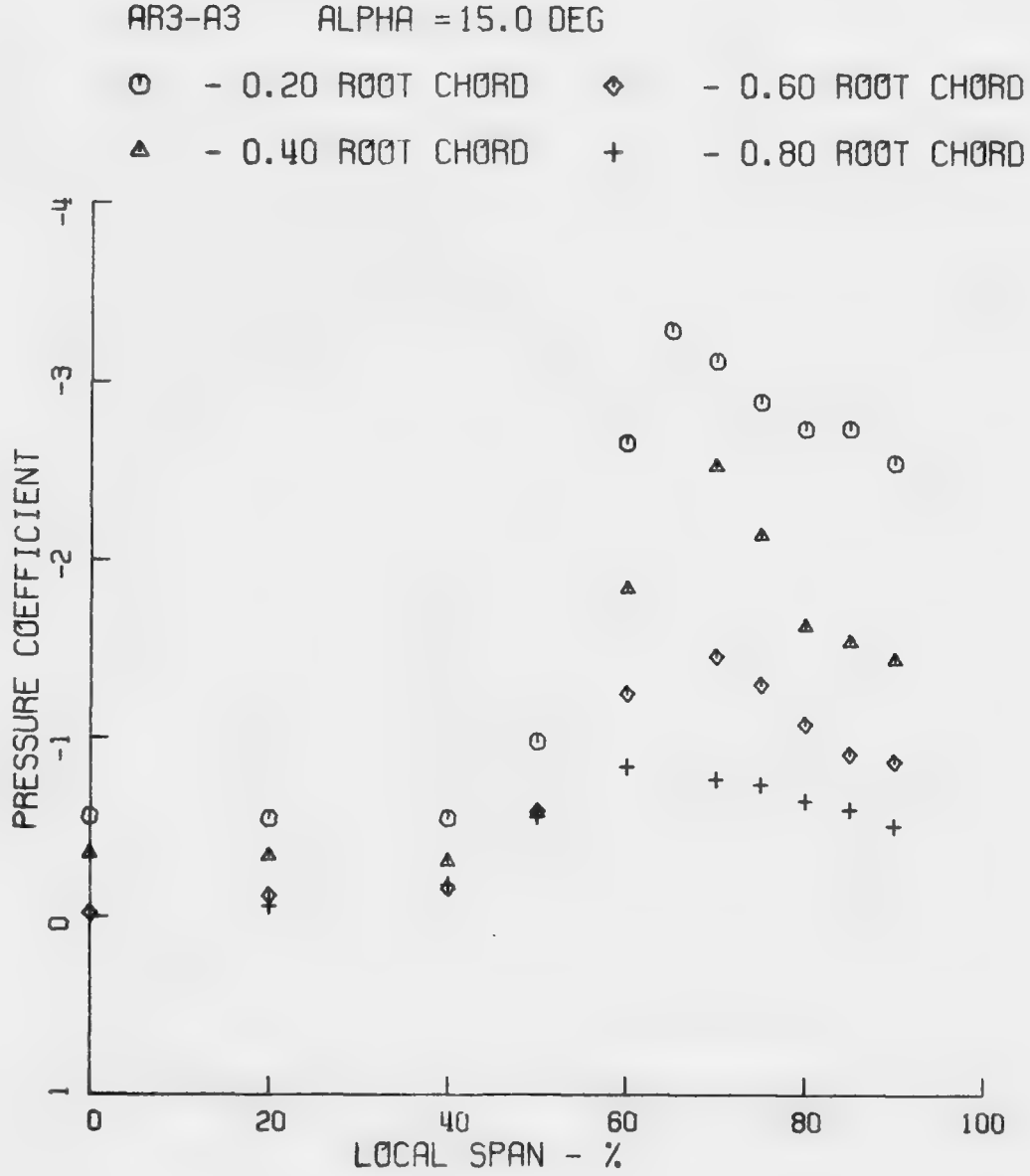
AR3-A3 ALPHA =15.0 DEG
- 0.20 ROOT CHORD
- 0.40 ROOT CHORD
- 0.60 ROOT CHORD
- 0.80 ROOT CHORD
PRESSURE COEFFICIENT
-4
-3
-2
-1
0
1
0
20
40
60
80
100
LOCAL SPAN - %

FIG. 5e

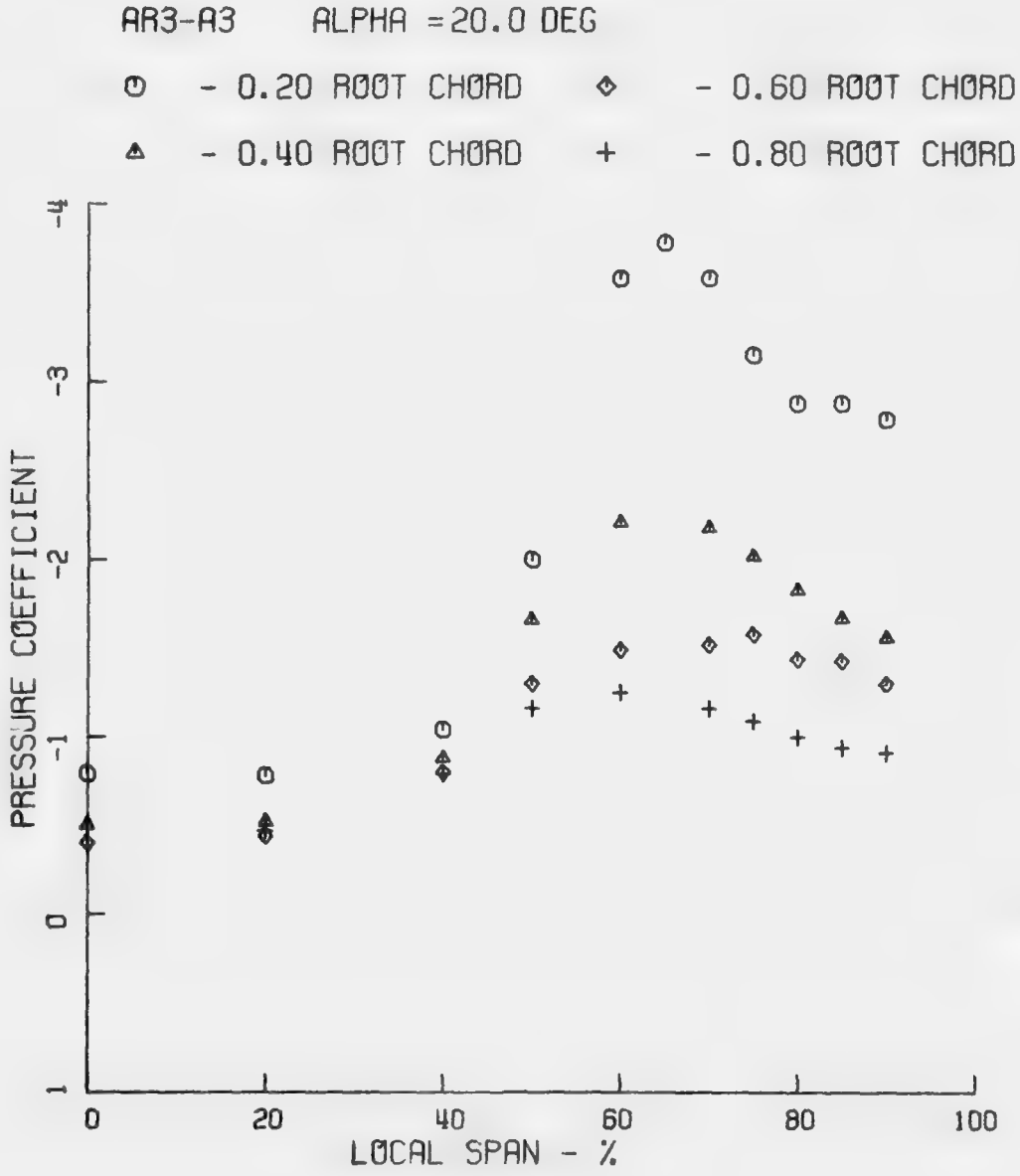
AR3-A3 ALPHA = 20.0 DEG
- 0.20 ROOT CHORD
- 0.40 ROOT CHORD
- 0.60 ROOT CHORD
- 0.80 ROOT CHORD
PRESSURE COEFFICIENT
-4
-3
-2
-1
0
1
0
20
40
60
80
100
LOCAL SPAN - %

FIG. 5f

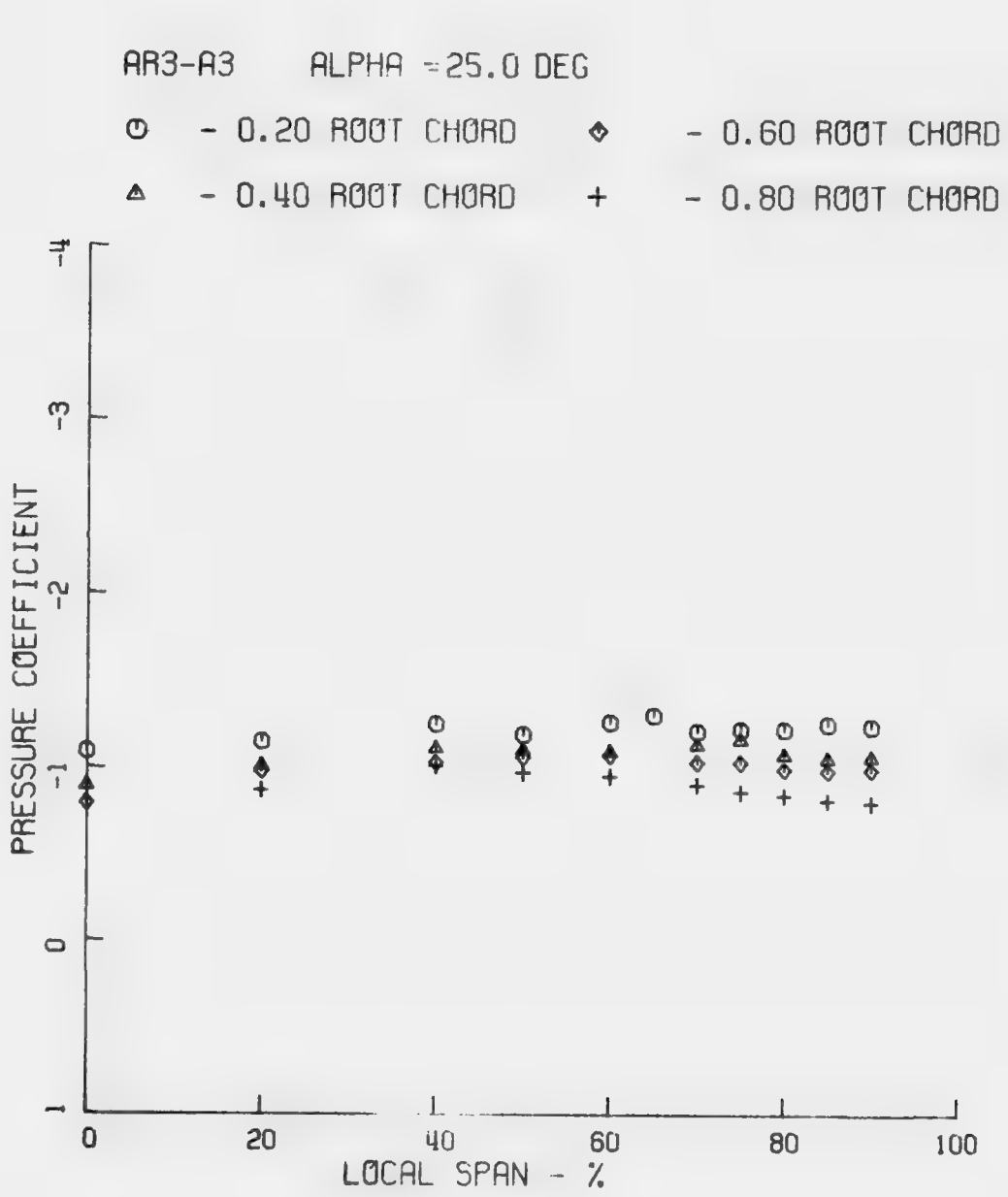
AR3-A3 ALPHA =25.0 DEG
- 0.20 ROOT CHORD
- 0.40 ROOT CHORD
- 0.60 ROOT CHORD
- 0.80 ROOT CHORD
PRESSURE COEFFICIENT
-4
-3
-2
-1
0
1
0
20
40
60
80
100
LOCAL SPAN - %

FIG. 5g

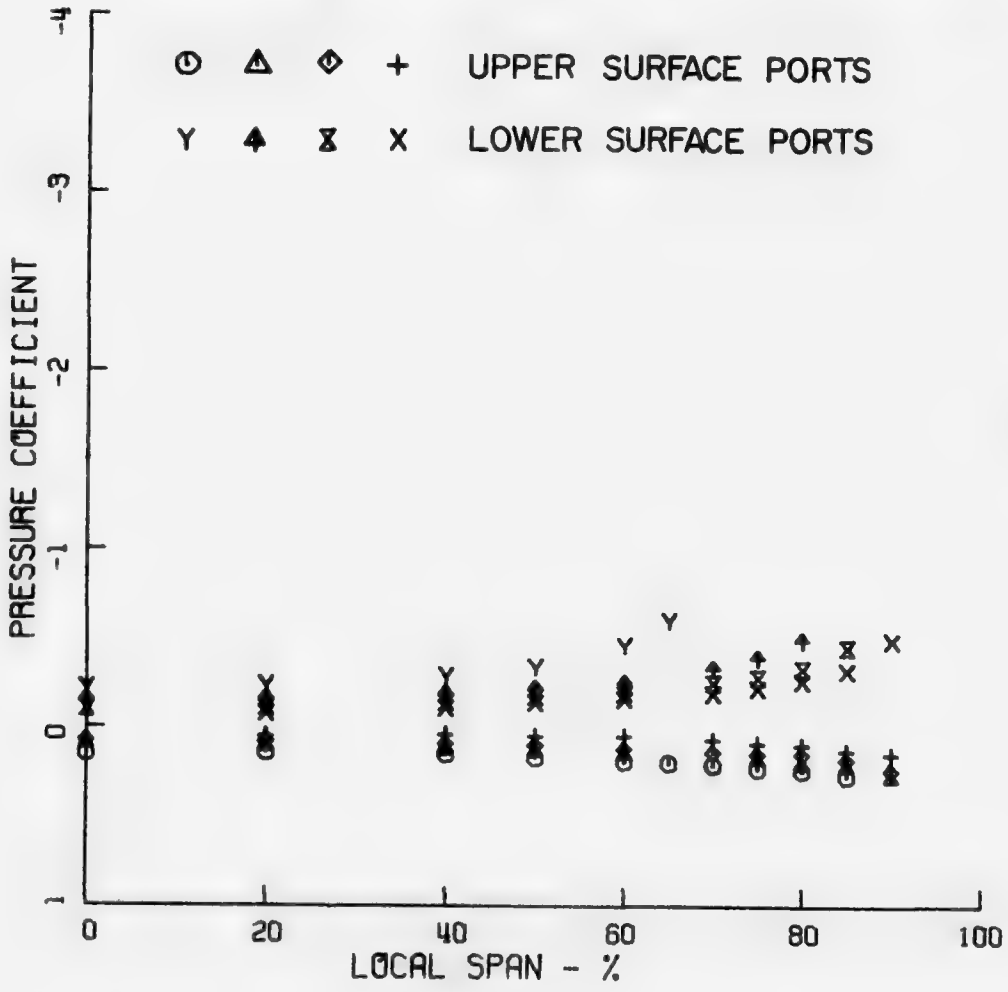

FIG. 6a PRESSURE DISTRIBUTION OVER AR4 WING

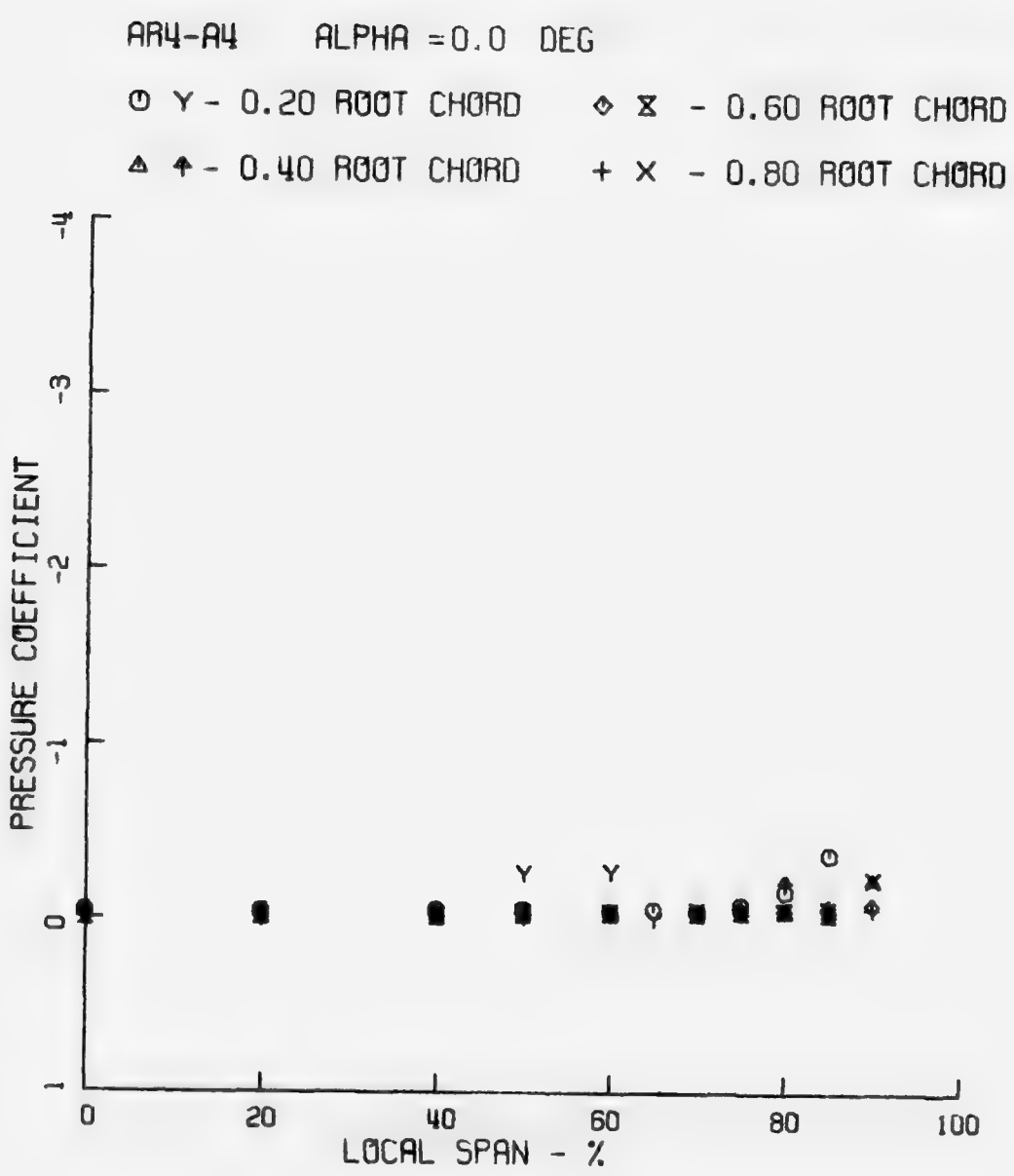
AR4-A4 ALPHA =0.0 DEG
Y - 0.20 ROOT CHORD
- 0.40 ROOT CHORD
- 0.60 ROOT CHORD
- 0.80 ROOT CHORD
PRESSURE COEFFICIENT
-4
-3
-2
-1
0
1
0
20
40
60
80
100
LOCAL SPAN - %

FIG. 6b

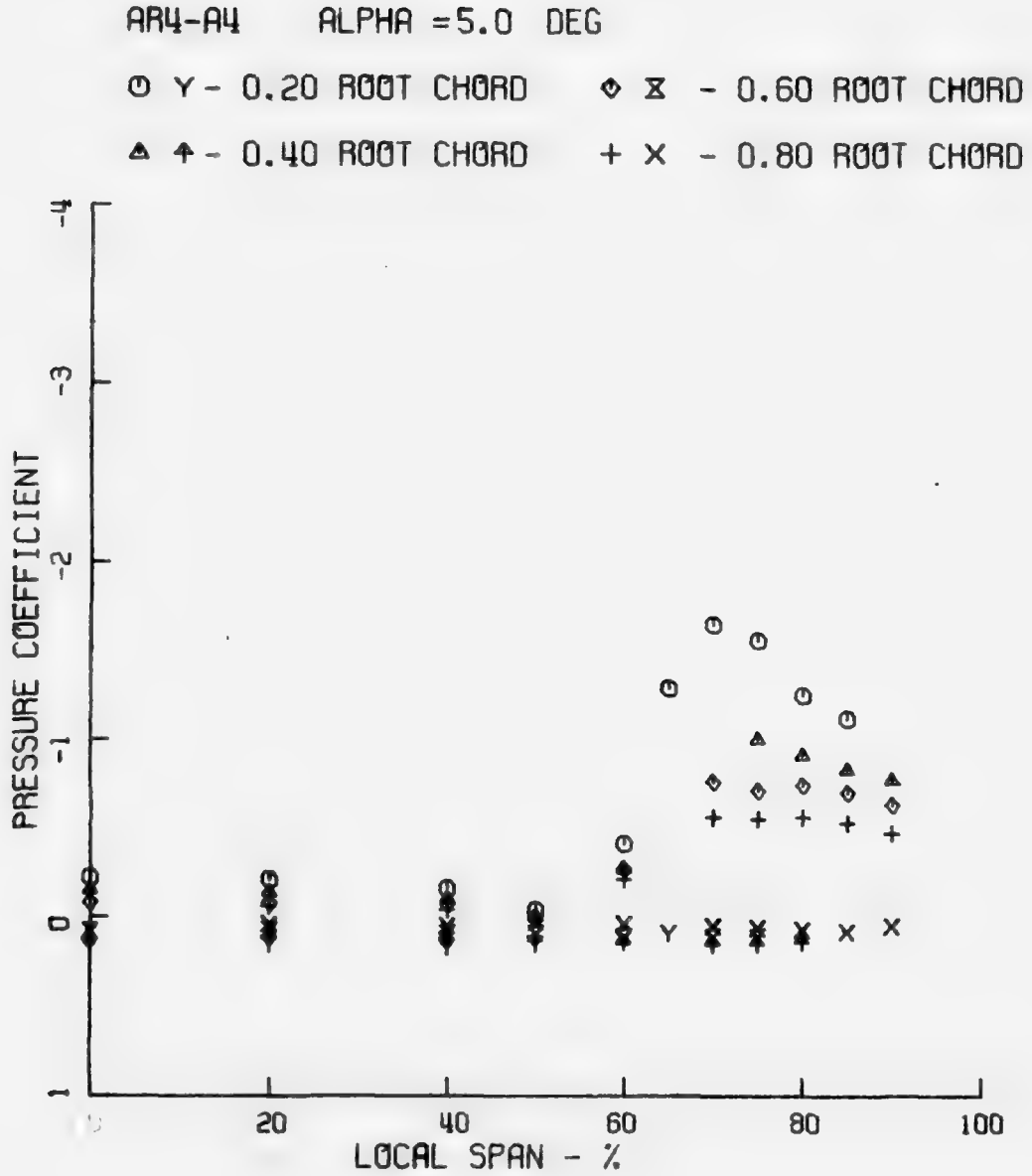
AR4-A4 ALPHA =5.0 DEG
Y - 0.20 ROOT CHORD
0.40 ROOT CHORD
0.60 ROOT CHORD
0.80 ROOT CHORD
PRESSURE COEFFICIENT
-4
-3
-2
-1
0
1
20
40
60
80
100
LOCAL SPAN - %

FIG. 6c

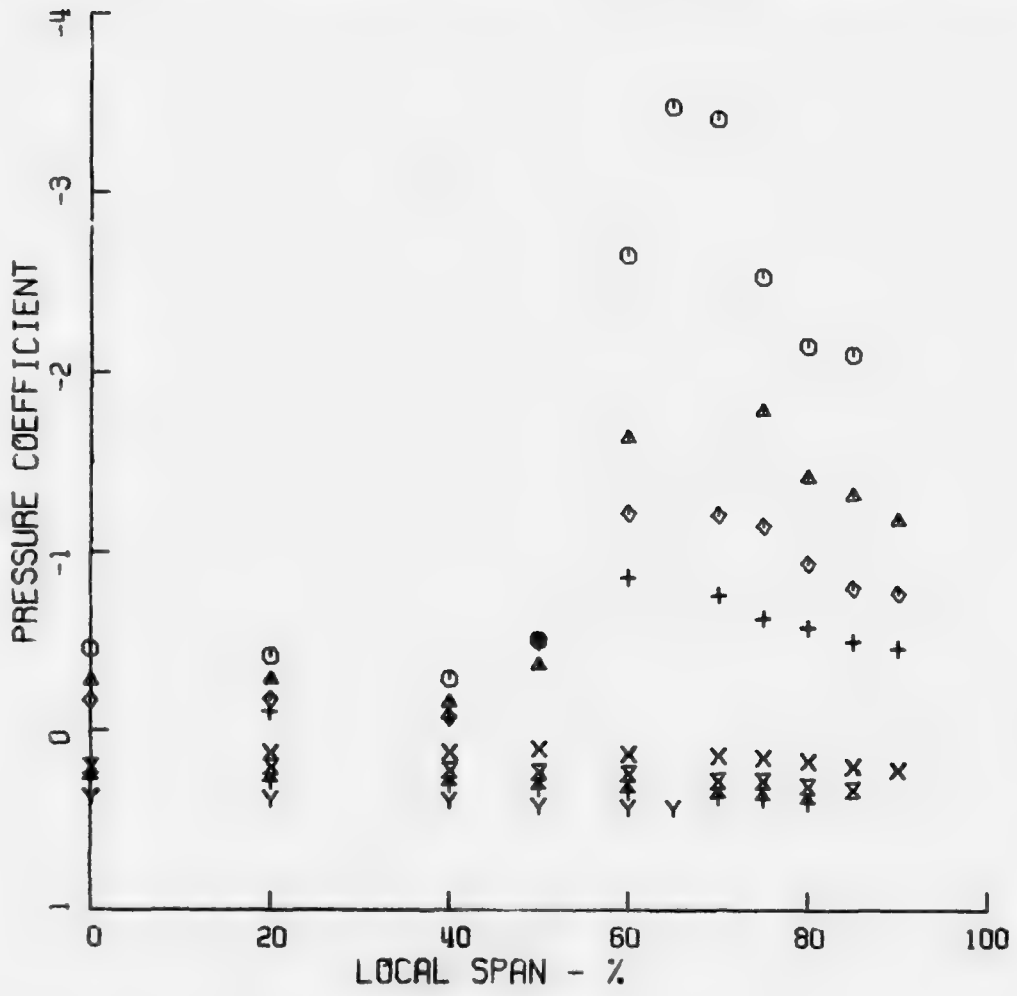
AR4-A4 ALPHA = 10.0 DEG
Y - 0.20 ROOT CHORD
0.40 ROOT CHORD
0.60 ROOT CHORD
0.80 ROOT CHORD
PRESSURE COEFFICIENT
-4
-3
-2
-1
0
1
0
20
40
60
80
100
LOCAL SPAN - %

FIG. 6d

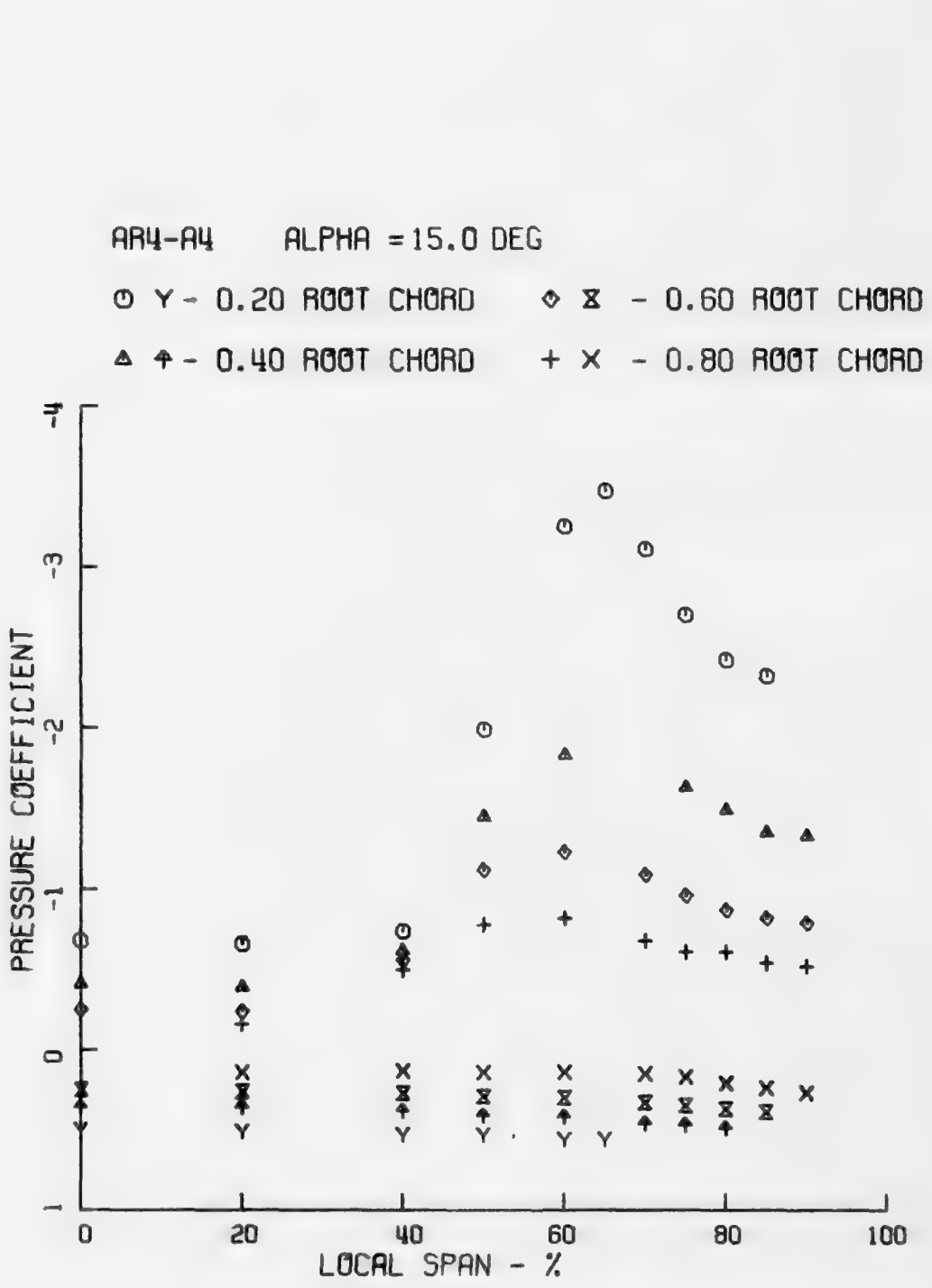
AR4-A4 ALPHA =15.0 DEG
Y - 0.20 ROOT CHORD
X - 0.60 ROOT CHORD
- 0.40 ROOT CHORD
X - 0.80 ROOT CHORD
PRESSURE COEFFICIENT
-4
-3
-2
-1
0
1
0
20
40
60
80
100
LOCAL SPAN - %

FIG. 6e

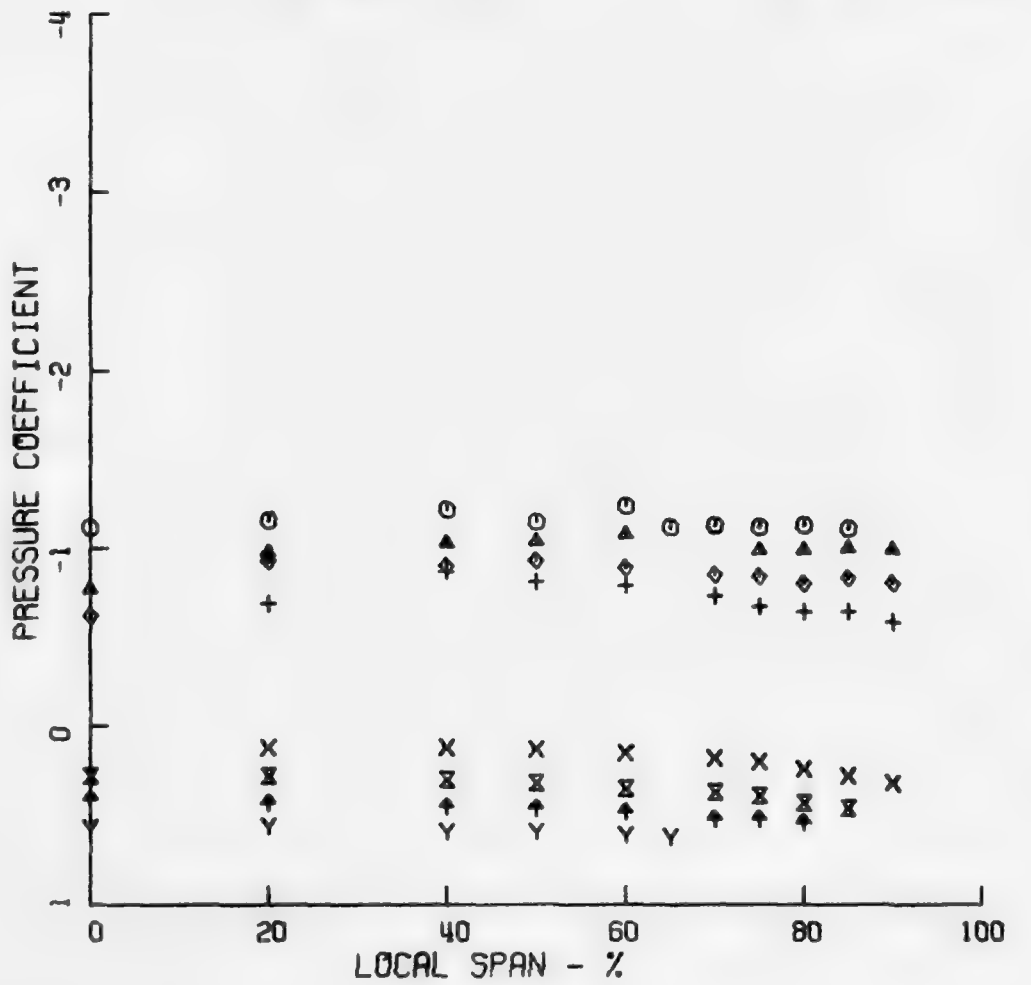
AR4-A4 ALPHA =20.0 DEG
Y - 0.20 ROOT CHORD
- 0.40 ROOT CHORD
- 0.60 ROOT CHORD
- 0.80 ROOT CHORD
PRESSURE COEFFICIENT
-4
-3
-2
-1
0
1
0
20
40
60
80
100
LOCAL SPAN - %

FIG. 6f

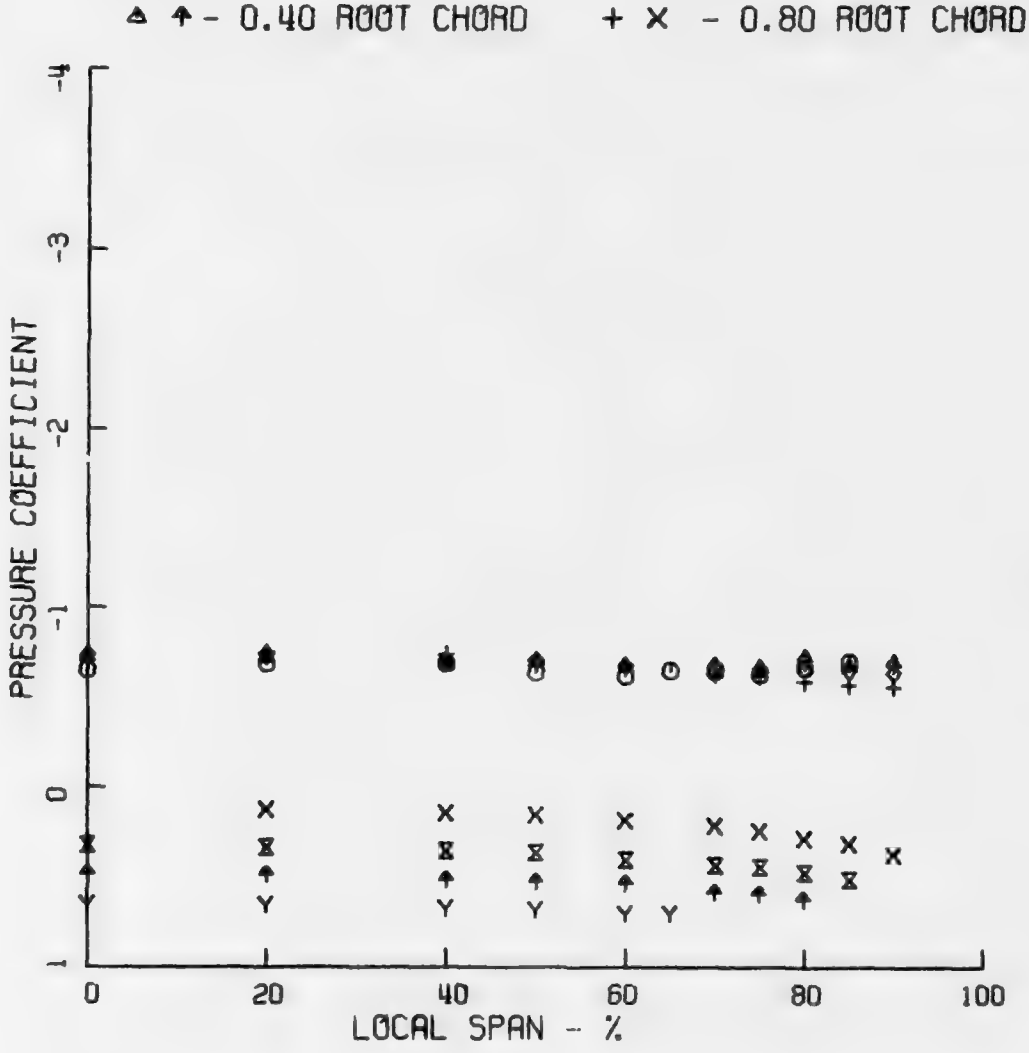
AR4-A4 ALPHA =25.0 DEG
Y - 0.20 ROOT CHORD
- 0.40 ROOT CHORD
- 0.60 ROOT CHORD
- 0.80 ROOT CHORD
PRESSURE COEFFICIENT
-4
-3
-2
-1
0
1
0
20
40
60
80
100
LOCAL SPAN - %

FIG. 6g

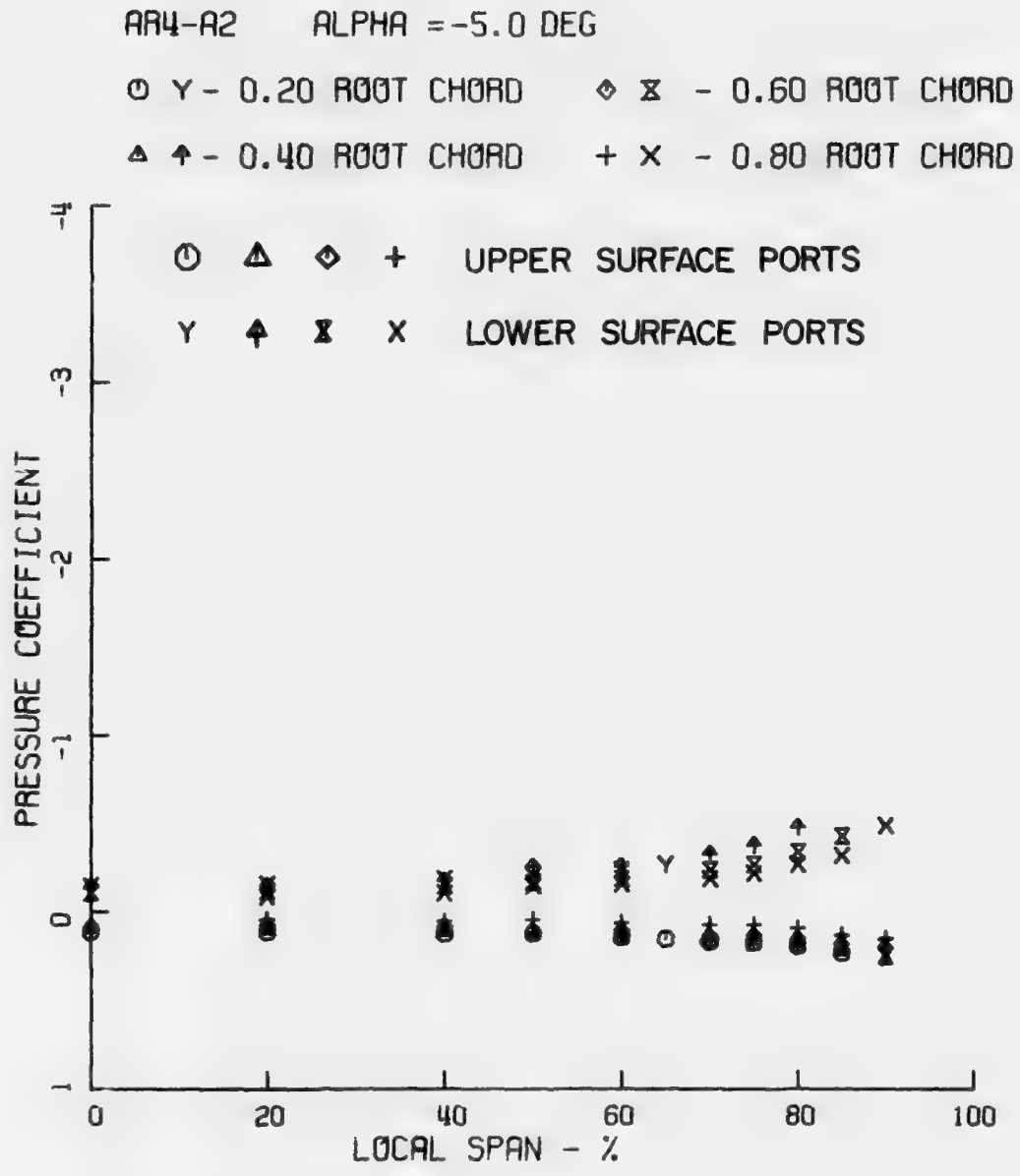

FIG. 7a PRESSURE DISTRIBUTION OVER AR4-A2 WING

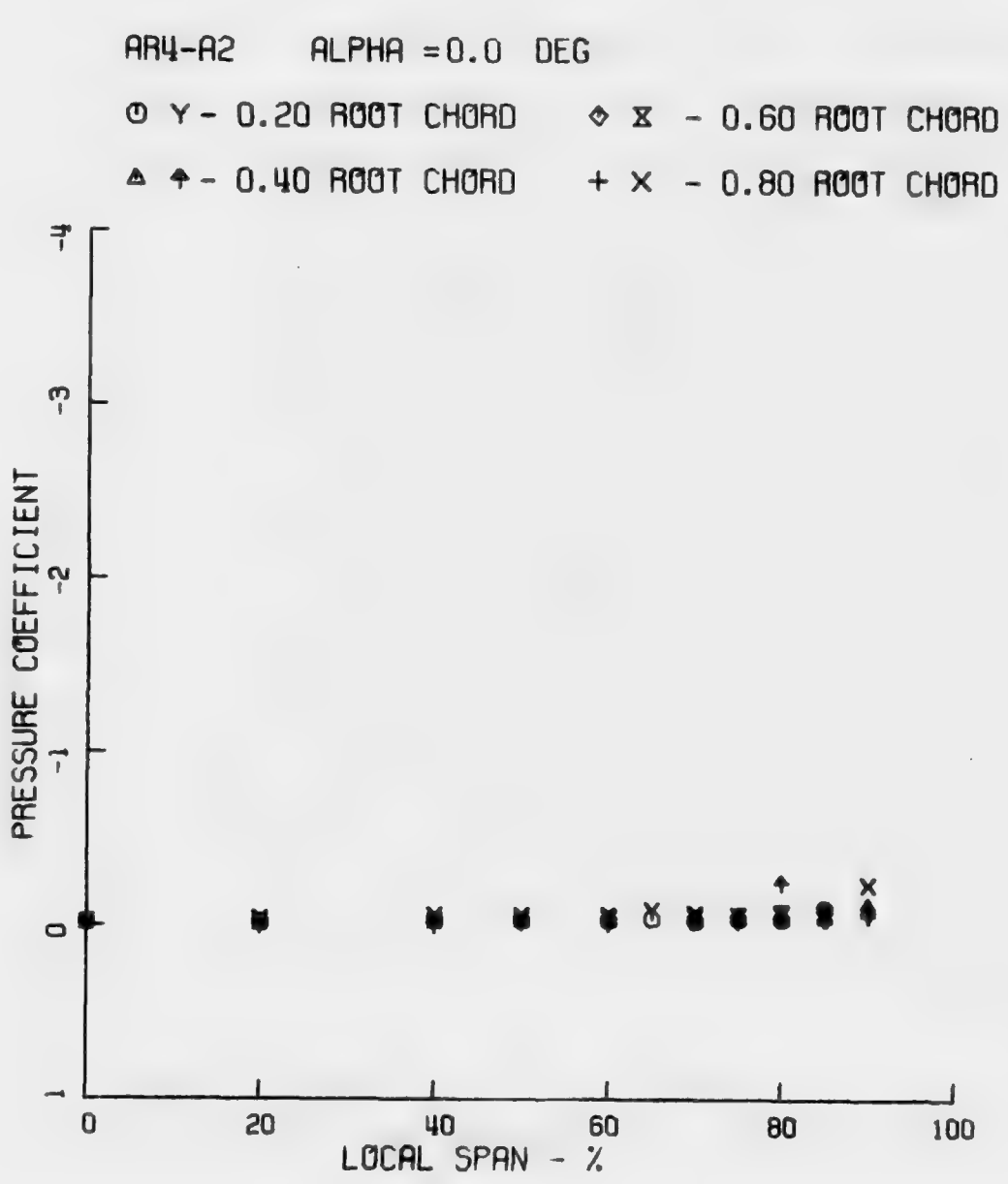
AR4-A2 ALPHA =0.0 DEG
Y - 0.20 ROOT CHORD
X - 0.60 ROOT CHORD
- 0.40 ROOT CHORD
X - 0.80 ROOT CHORD
PRESSURE COEFFICIENT
-4
-3
-2
-1
0
1
0
20
40
60
80
100
LOCAL SPAN - %

FIG. 7b

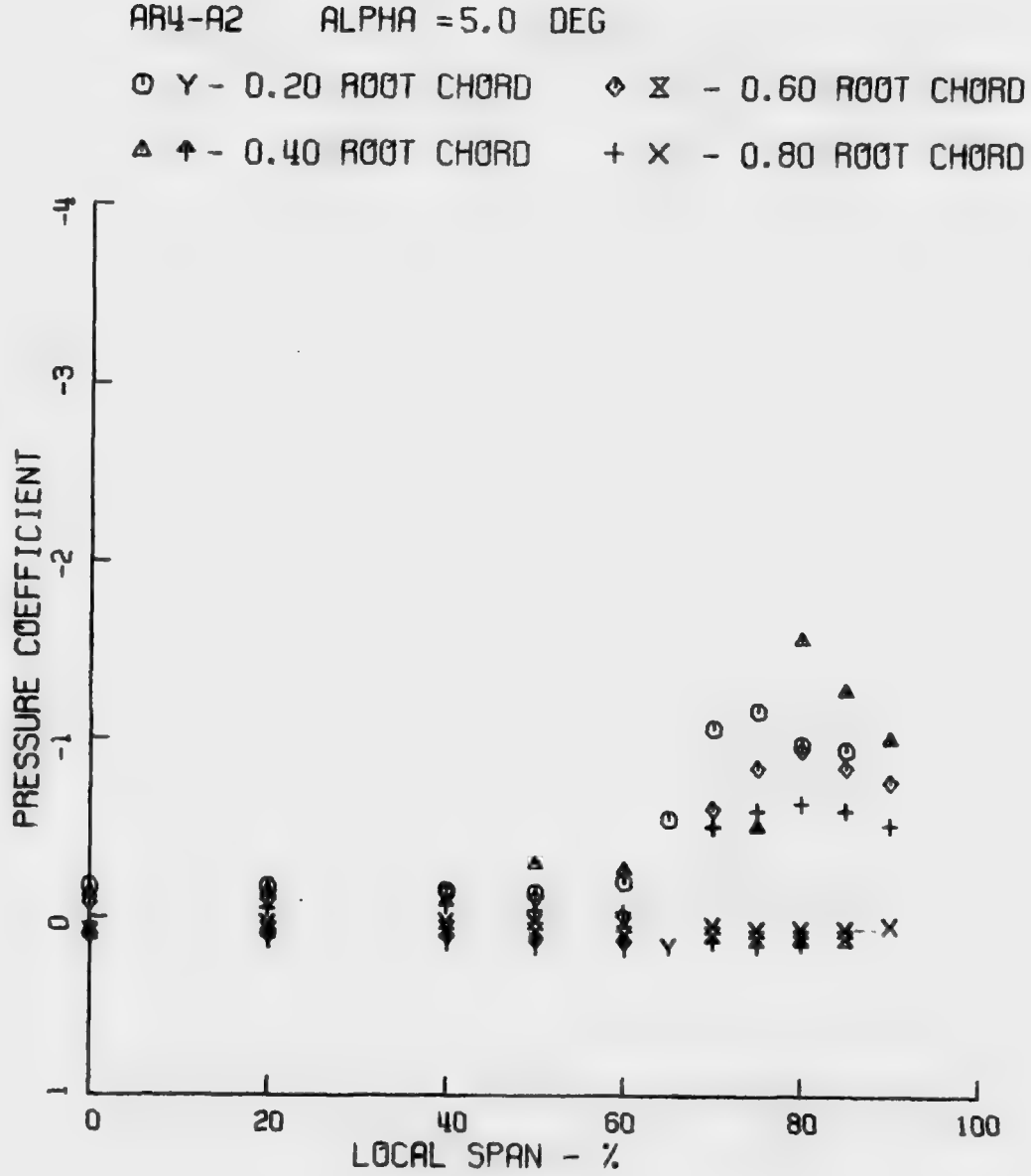
AR4-A2 ALPHA =5.0 DEG
Y - 0.20 ROOT CHORD
0.60 ROOT CHORD
0.40 ROOT CHORD
0.80 ROOT CHORD
PRESSURE COEFFICIENT
-4
-3
-2
-1
0
1
0
20
40
60
80
100
LOCAL SPAN - %

FIG. 7c

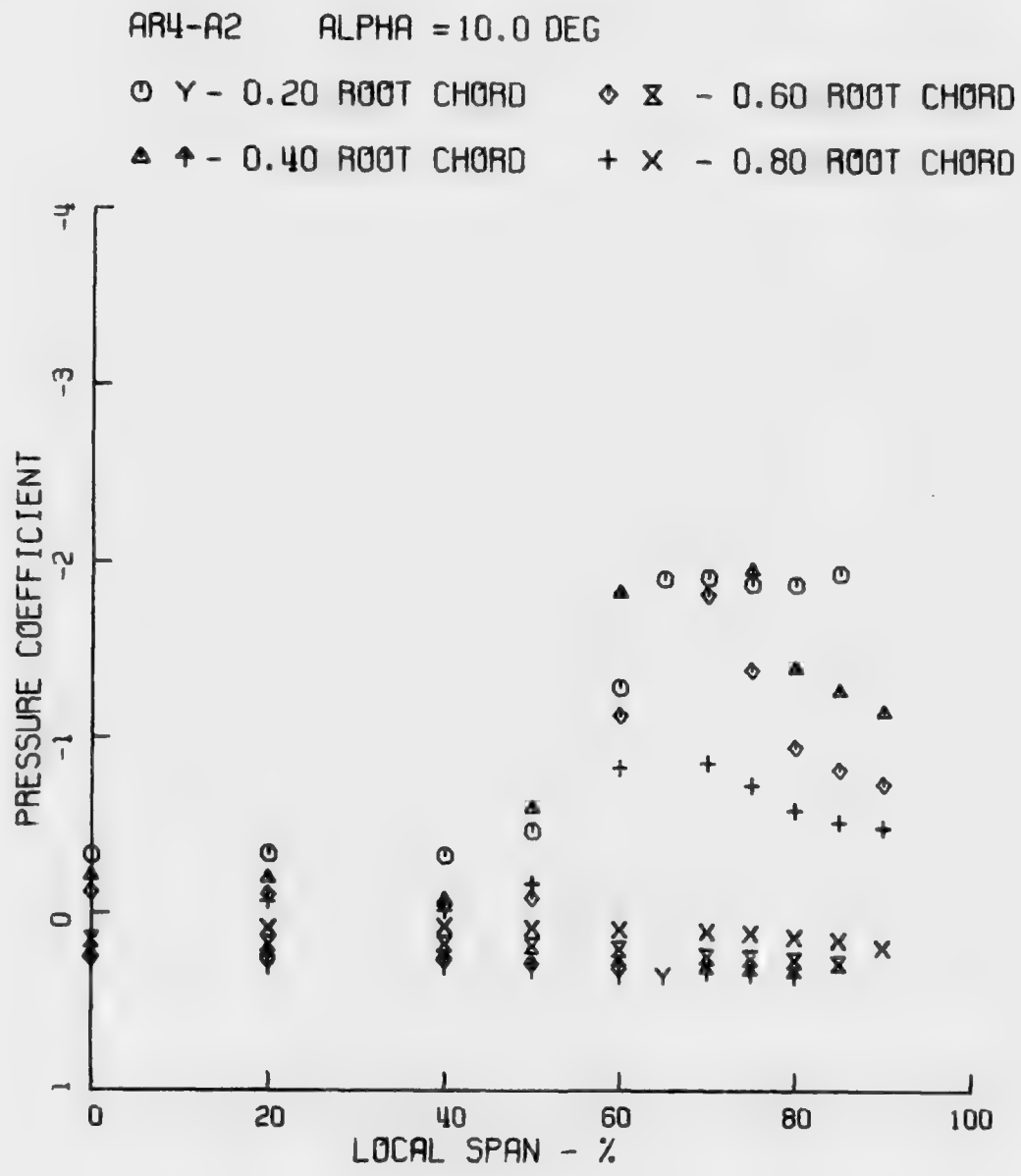
AR4-A2 ALPHA = 10.0 DEG
Y - 0.20 ROOT CHORD
0.60 ROOT CHORD
0.40 ROOT CHORD
0.80 ROOT CHORD
PRESSURE COEFFICIENT
-4
-3
-2
-1
0
1
0
20
40
60
80
100
LOCAL SPAN - %

FIG. 7d

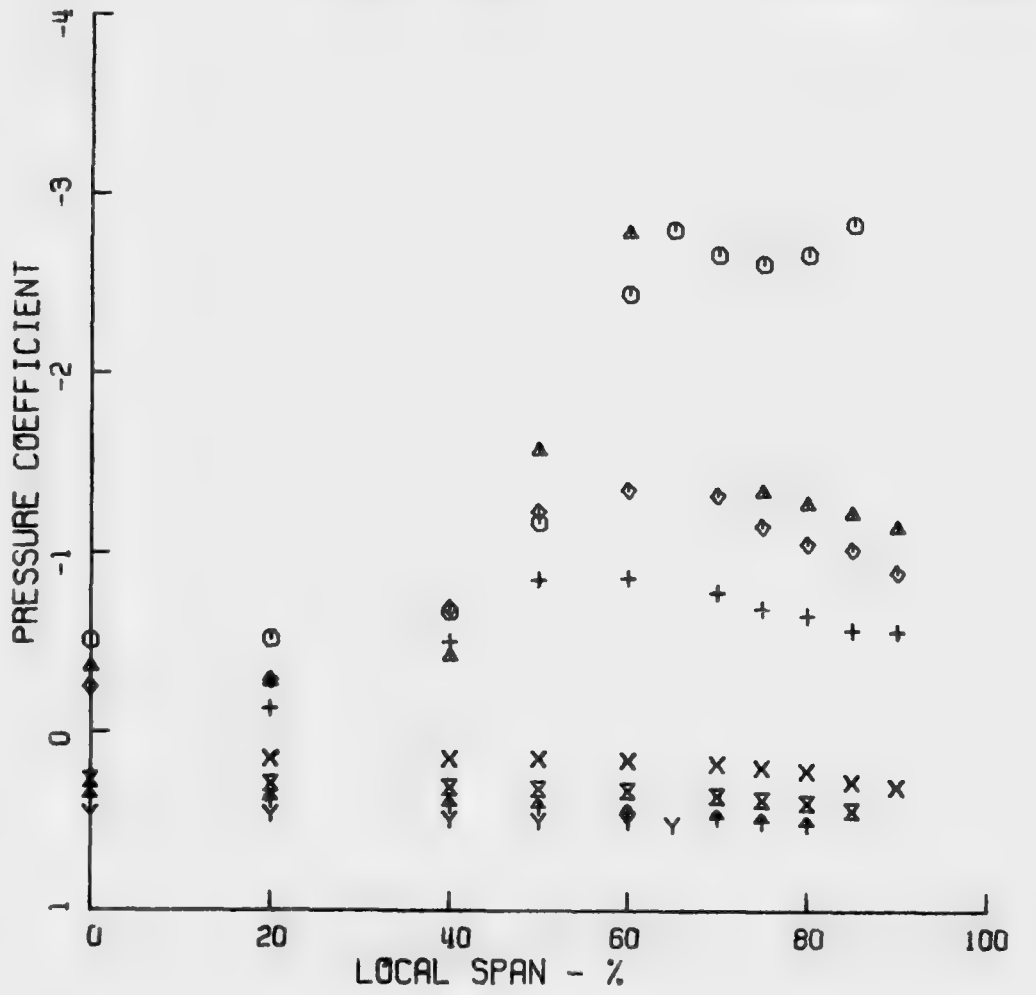
AR4-A2 ALPHA = 15.0 DEG
Y - 0.20 ROOT CHORD
0.60 ROOT CHORD
0.40 ROOT CHORD
0.80 ROOT CHORD
PRESSURE COEFFICIENT
-4
-3
-2
-1
0
1
0
20
40
60
80
100
LOCAL SPAN - %
Y

FIG. 7e

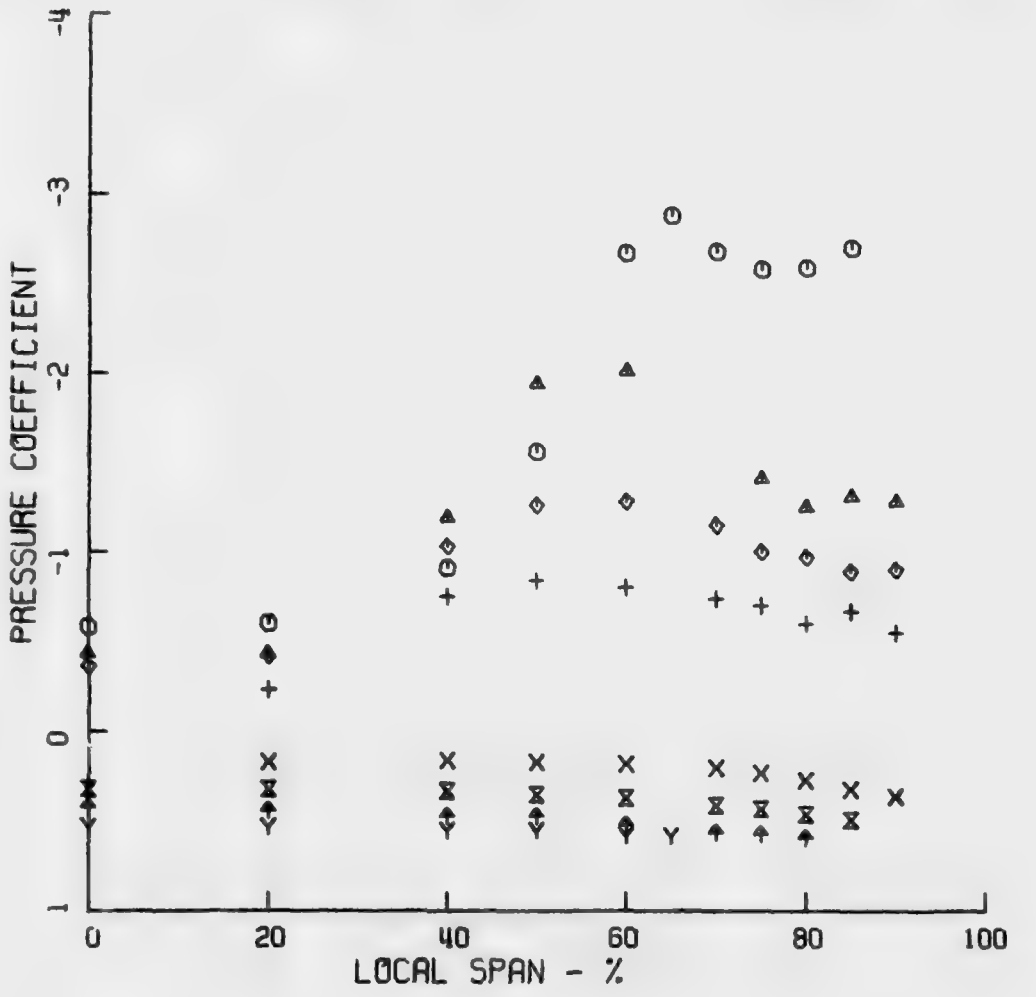
AR4-A2 ALPHA =20.0 DEG
Y - 0.20 ROOT CHORD
0.60 ROOT CHORD
0.40 ROOT CHORD
0.80 ROOT CHORD
PRESSURE COEFFICIENT
-4
-3
-2
-1
0
1
0
20
40
60
80
100
LOCAL SPAN - %

FIG. 7f

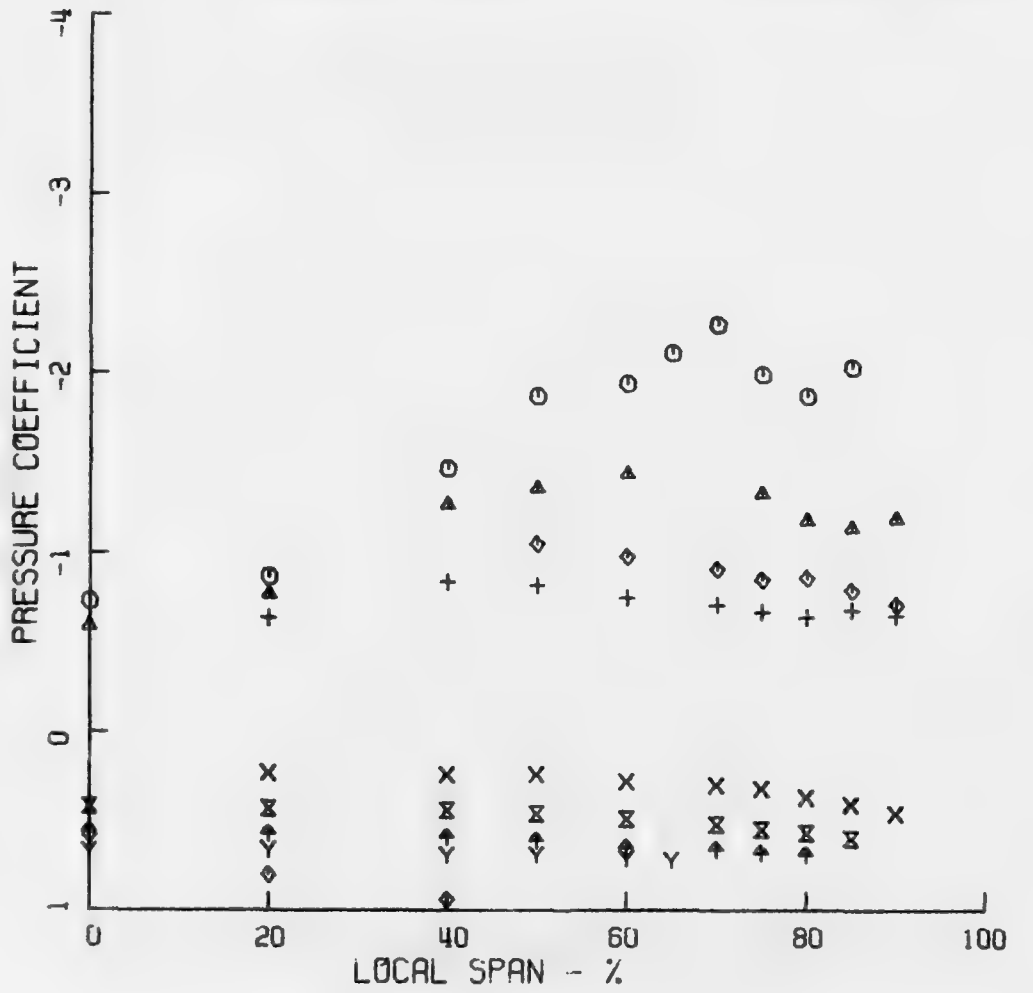
AR4-A2 ALPHA =25.0 DEG
Y - 0.20 ROOT CHORD
0.60 ROOT CHORD
0.40 ROOT CHORD
0.80 ROOT CHORD
PRESSURE COEFFICIENT
-4
-3
-2
-1
0
1
0
20
40
60
80
100
LOCAL SPAN - %

FIG. 7g

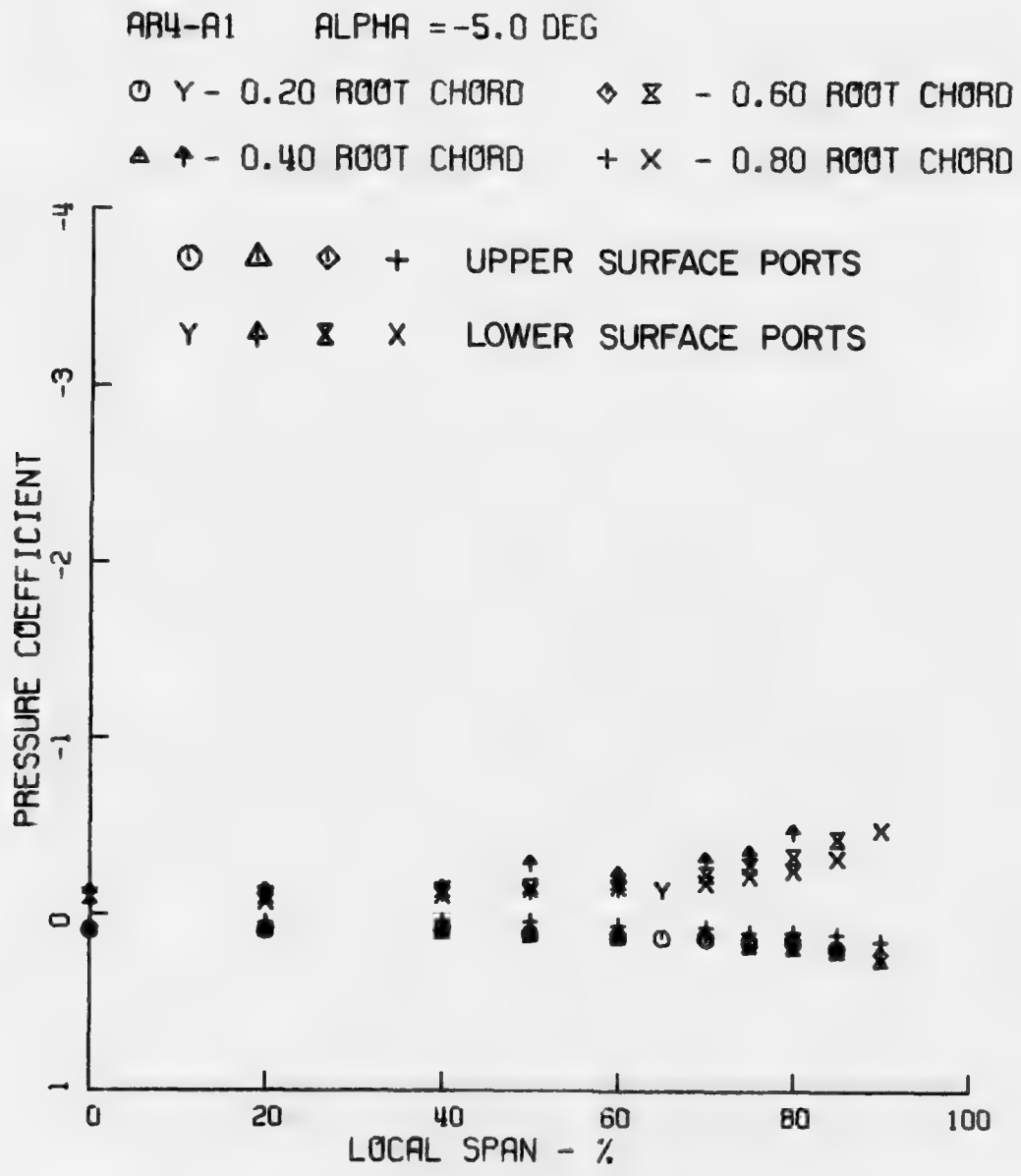

FIG. 8a PRESSURE DISTRIBUTION OVER AR2-A1 WING

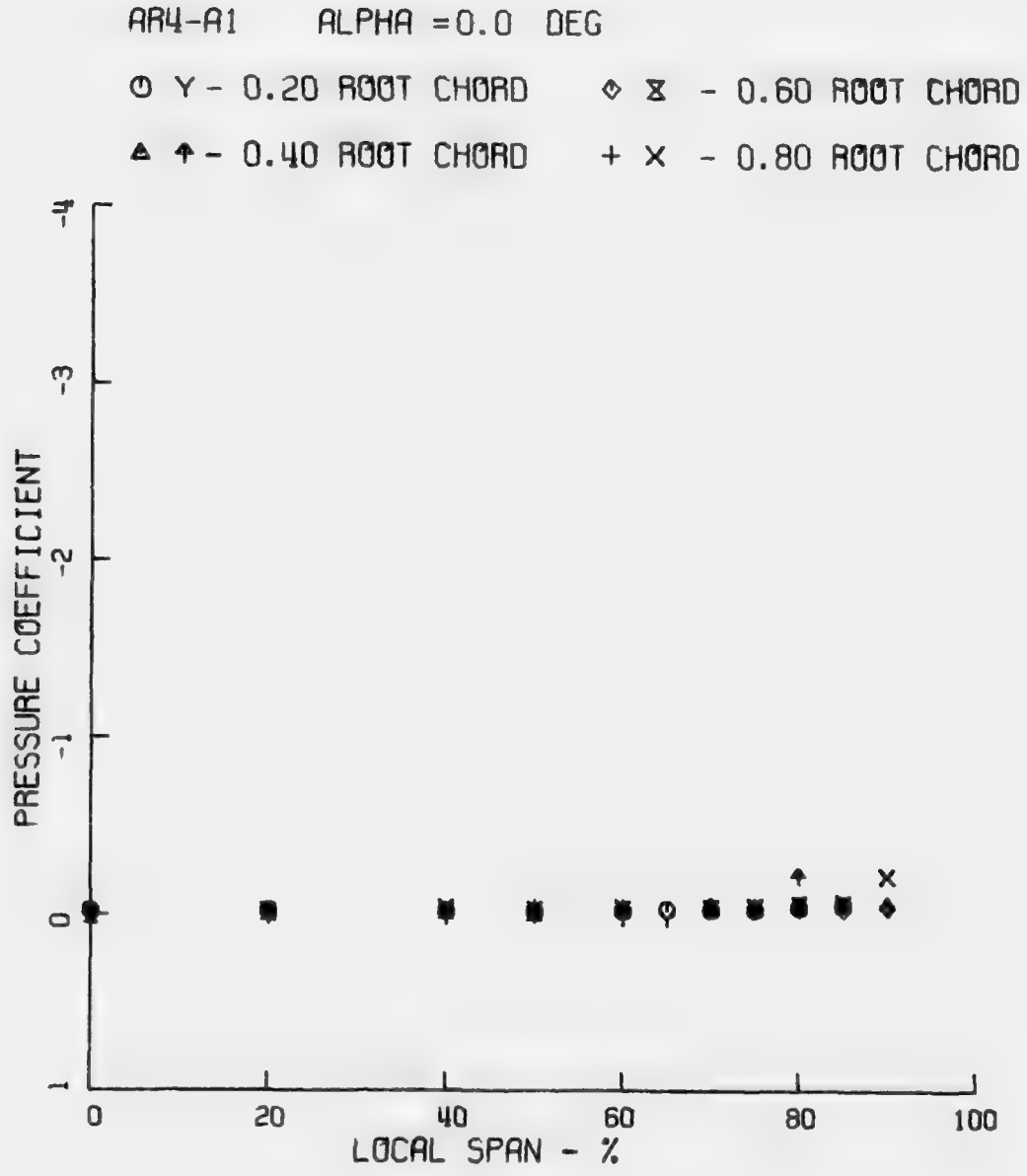
AR4-A1 ALPHA =0.0 DEG
Y - 0.20 ROOT CHORD
0.40 ROOT CHORD
0.60 ROOT CHORD
0.80 ROOT CHORD
PRESSURE COEFFICIENT
-4
-3
-2
-1
0
1
0
20
40
60
80
100
LOCAL SPAN - %

FIG. 8b

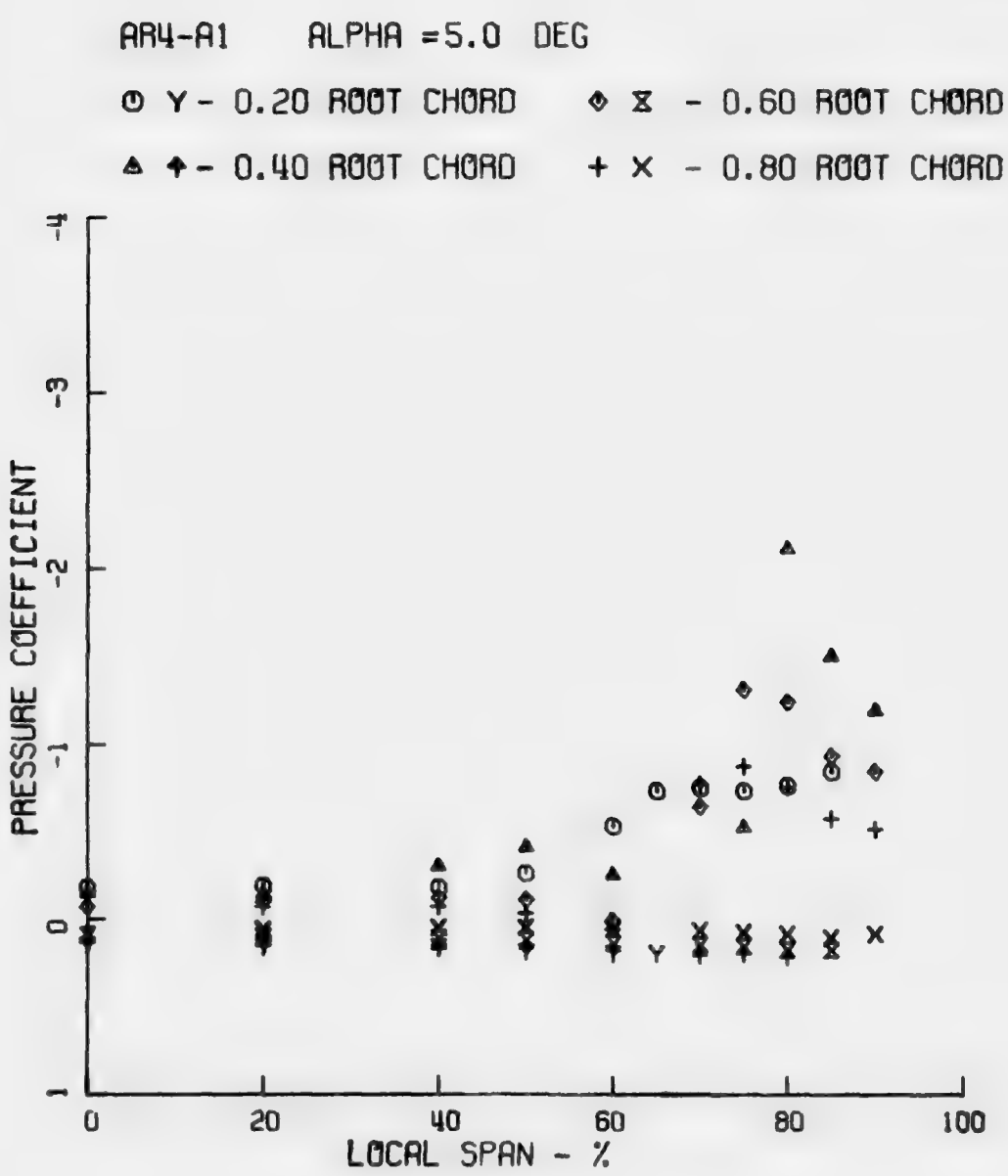
AR4-A1 ALPHA =5.0 DEG
Y - 0.20 ROOT CHORD
0.40 ROOT CHORD
0.60 ROOT CHORD
0.80 ROOT CHORD
PRESSURE COEFFICIENT
-4
-3
-2
-1
0
1
0
20
40
60
80
100
LOCAL SPAN - %

FIG. 8c

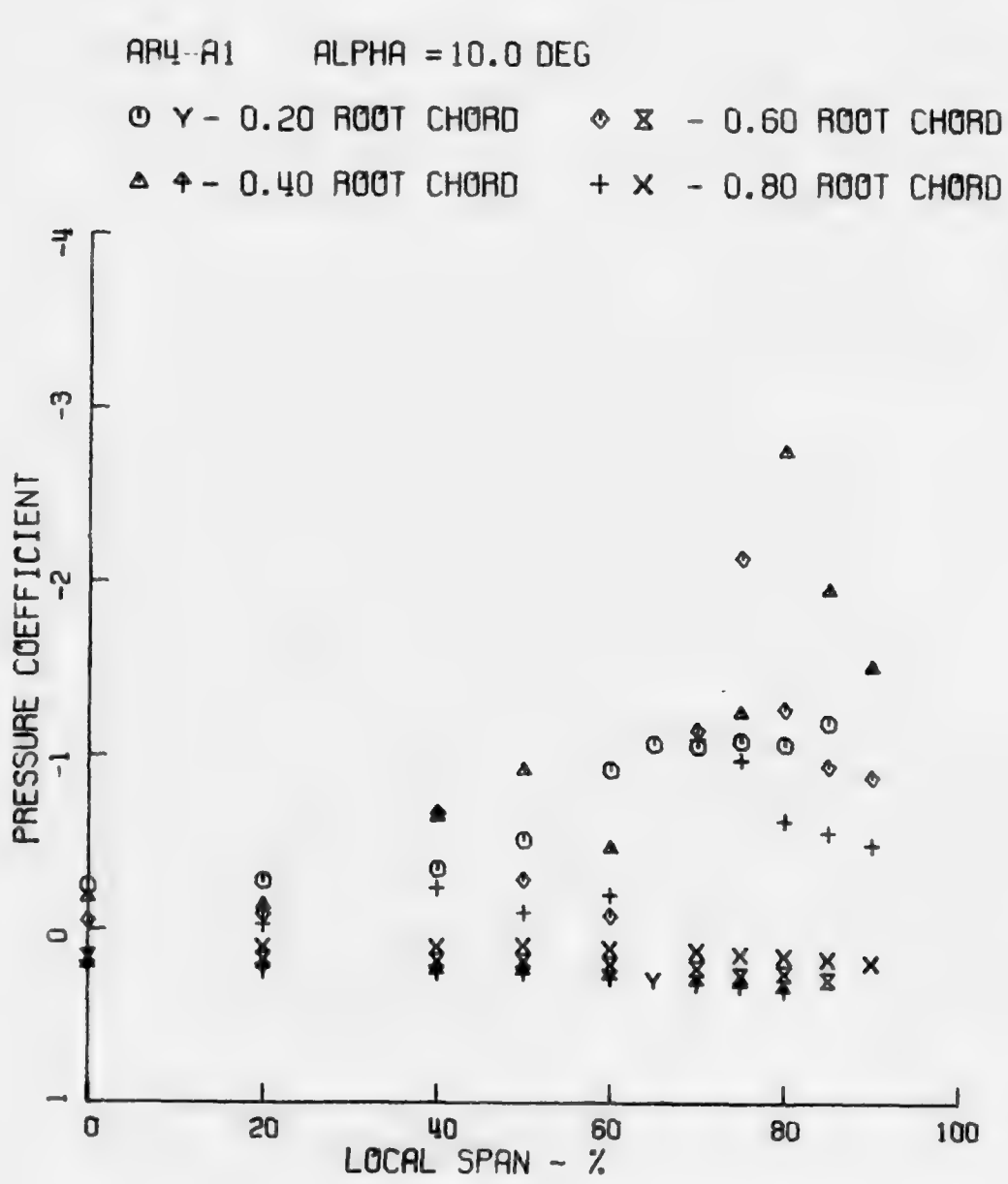
AR4-A1 ALPHA = 10.0 DEG
Y - 0.20 ROOT CHORD
0.40 ROOT CHORD
0.60 ROOT CHORD
0.80 ROOT CHORD
PRESSURE COEFFICIENT
-4
-3
-2
-1
0
1
0
20
40
60
80
100
LOCAL SPAN - %

FIG. 8d

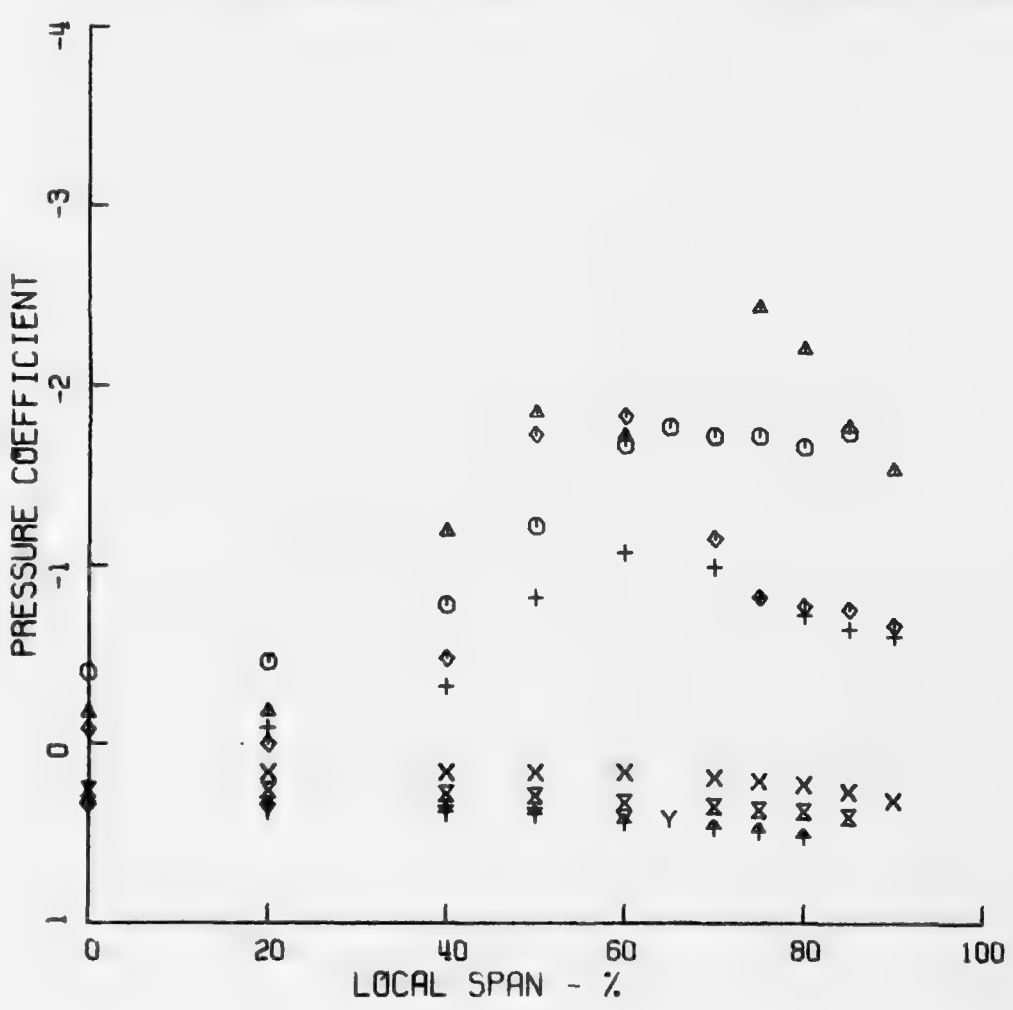
AR4-A1 ALPHA = 15.0 DEG
Y - 0.20 ROOT CHORD
0.40 ROOT CHORD
0.60 ROOT CHORD
0.80 ROOT CHORD
PRESSURE COEFFICIENT
-4
-3
-2
-1
0
1
0
20
40
60
80
100
LOCAL SPAN - %

FIG. 8e

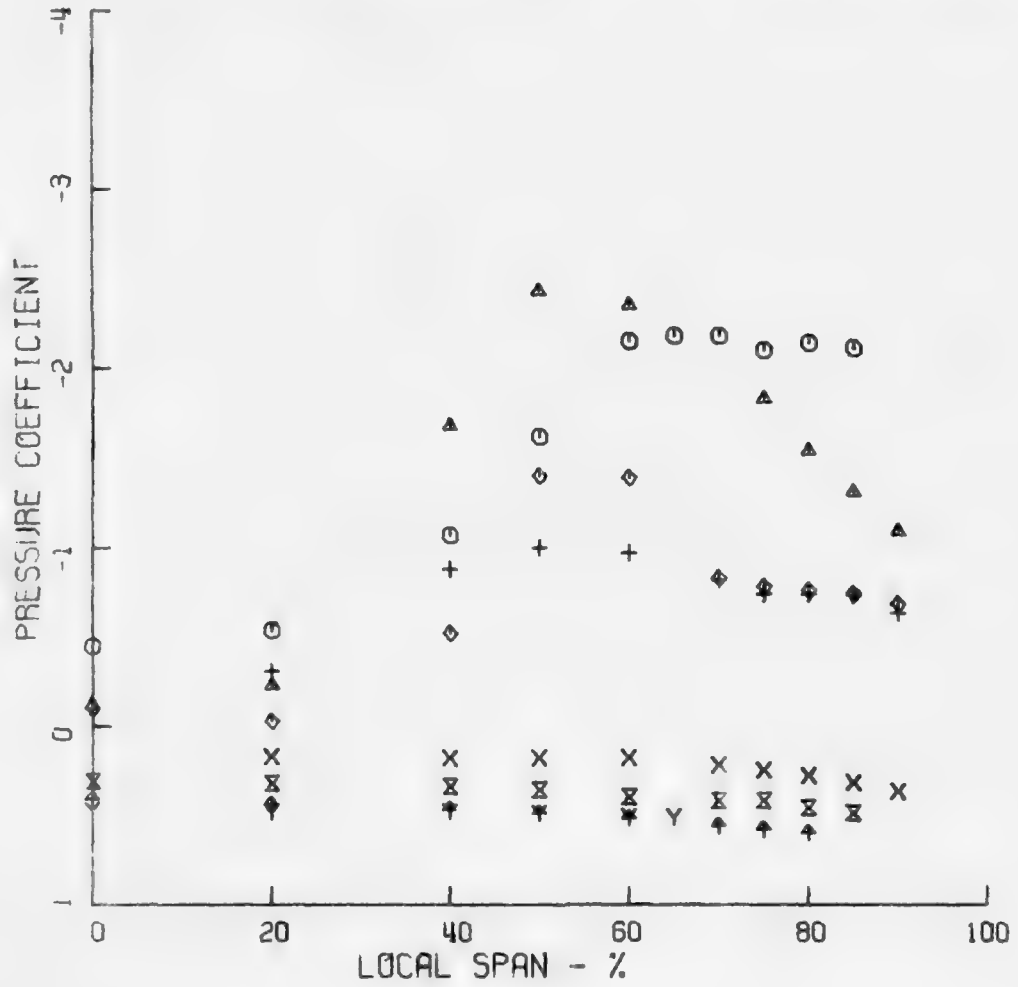
AR4-A1 ALPHA = 20.0 DEG
Y - 0.20 ROOT CHORD
0.40 ROOT CHORD
0.60 ROOT CHORD
0.80 ROOT CHORD
PRESSURE COEFFICIENT
-4
-3
-2
-1
0
1
0
20
40
60
80
100
LOCAL SPAN - %

FIG. 8f

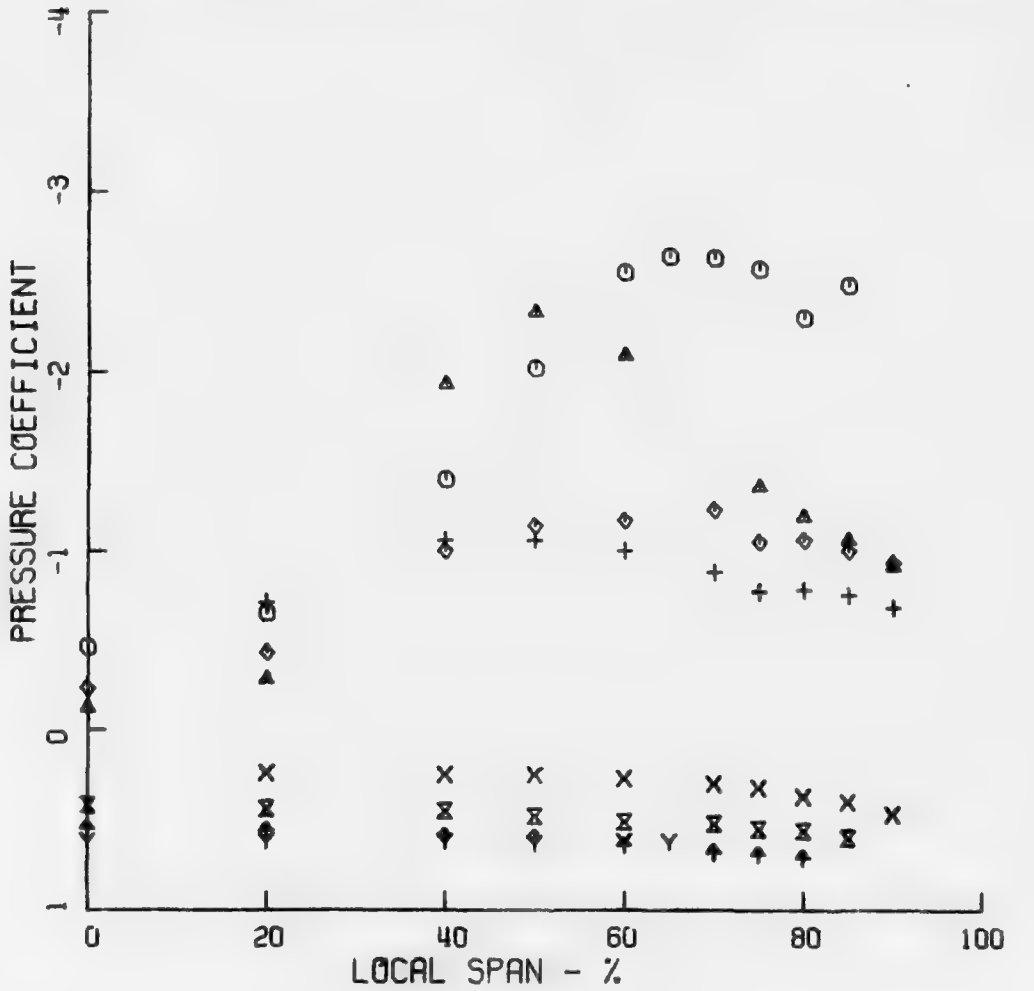
AR4-A1 ALPHA =25.0 DEG
Y - 0.20 ROOT CHORD
0.40 ROOT CHORD
0.60 ROOT CHORD
0.80 ROOT CHORD
PRESSURE COEFFICIENT
-4
-3
-2
-1
0
1
0
20
40
60
80
100
LOCAL SPAN - %

FIG. 8g

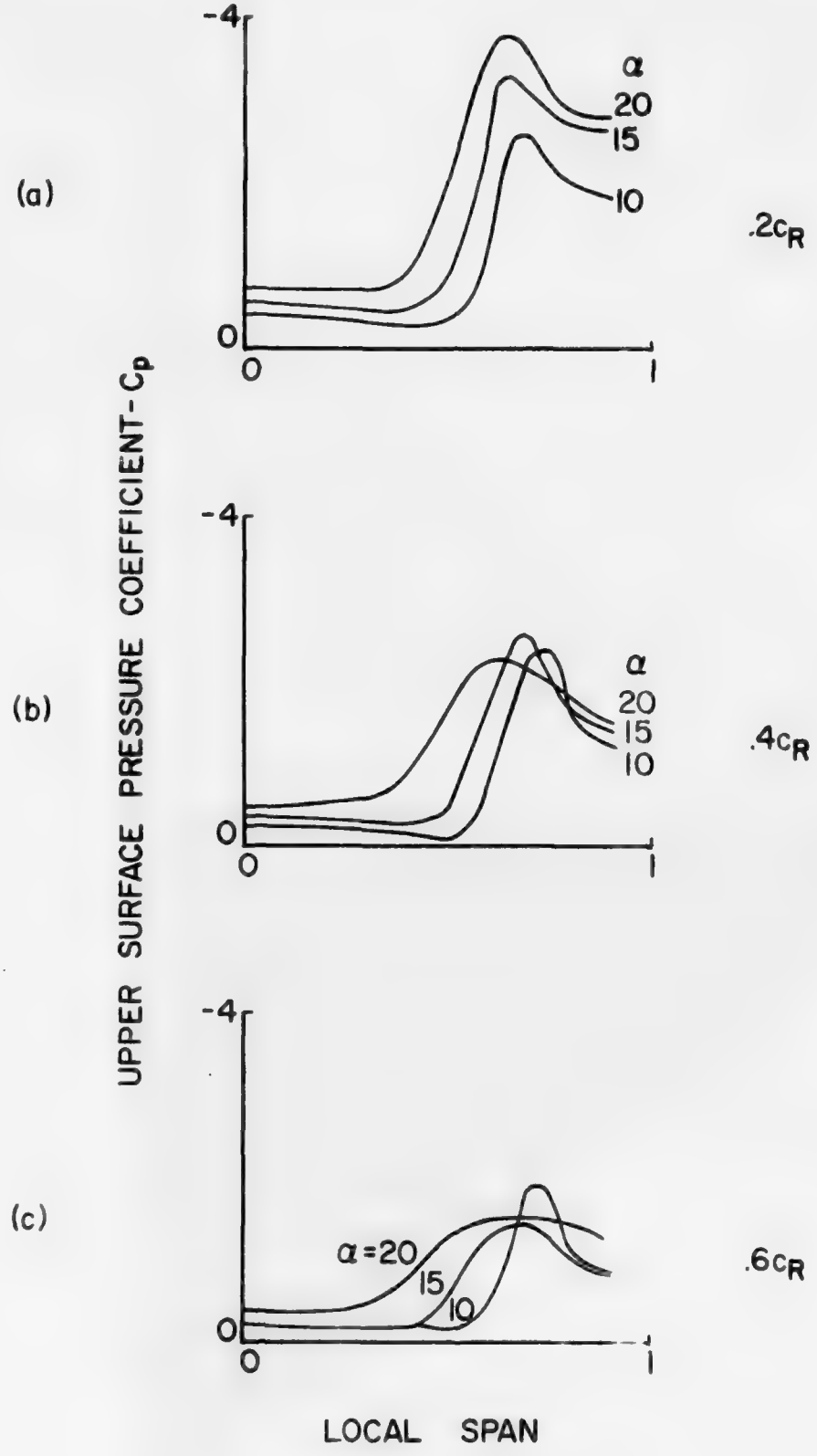

FIG. 9 EFFECT OF BURST ON PRESSURE DISTRIBUTION

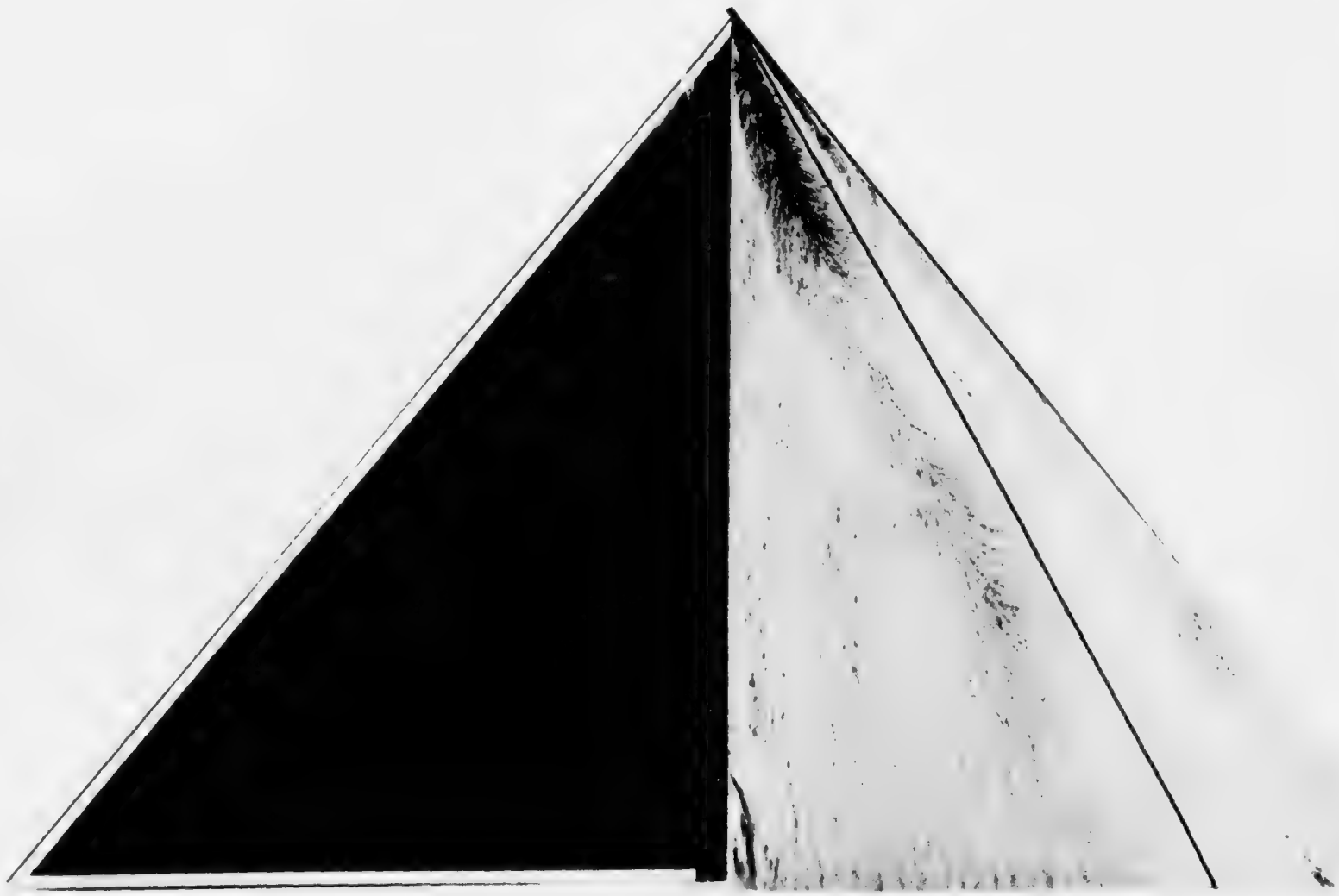

FIG. 10a SURFACE FLOW PATTERN AND VORTEX STRUCTURE OVER AR3 WING (α = 10°)

FIG. 10b $\alpha = 15°$

FIG. 10c $\alpha = 20°$

FIG. 10d $\alpha = 25°$

FIG. 11a SURFACE FLOW PATTERN AND VORTEX STRUCTURE OVER AR4 WING

FIG. 11b $\alpha = 10°$

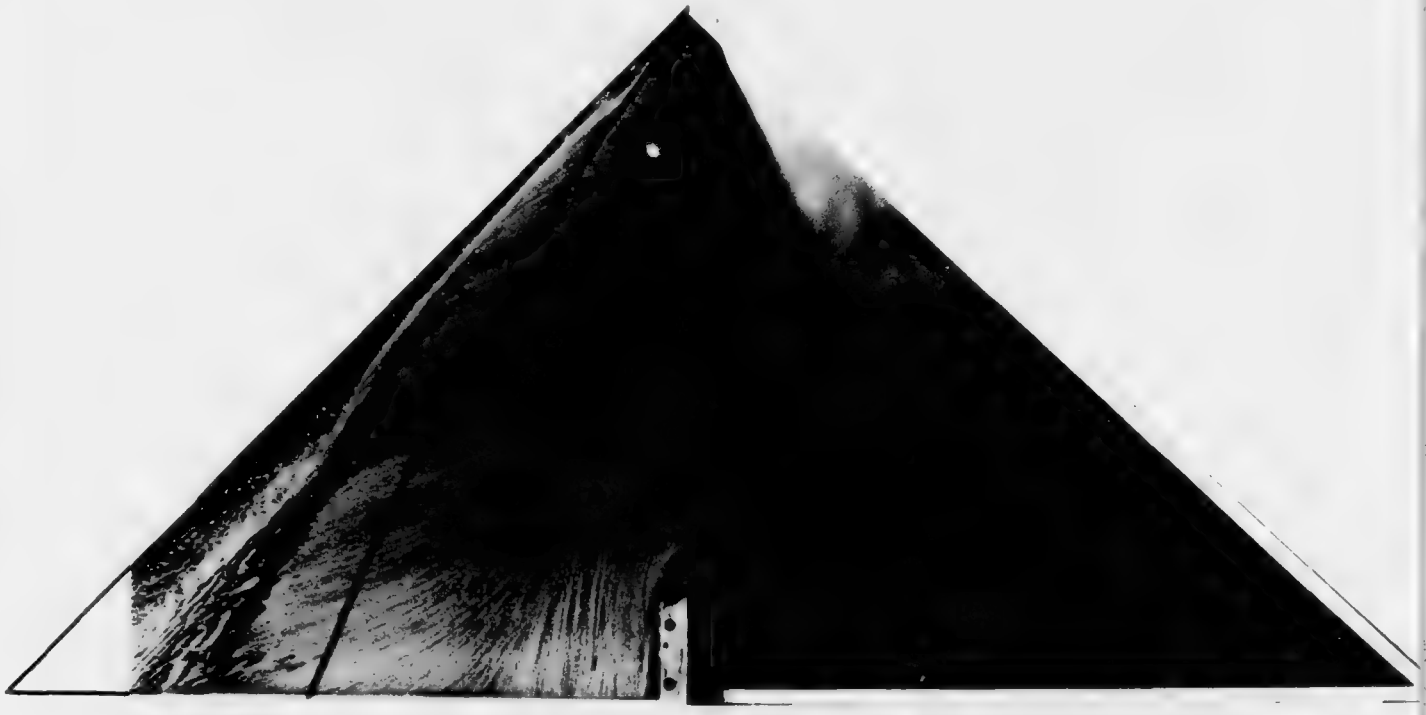

FIG. 11c $\alpha = 15°$

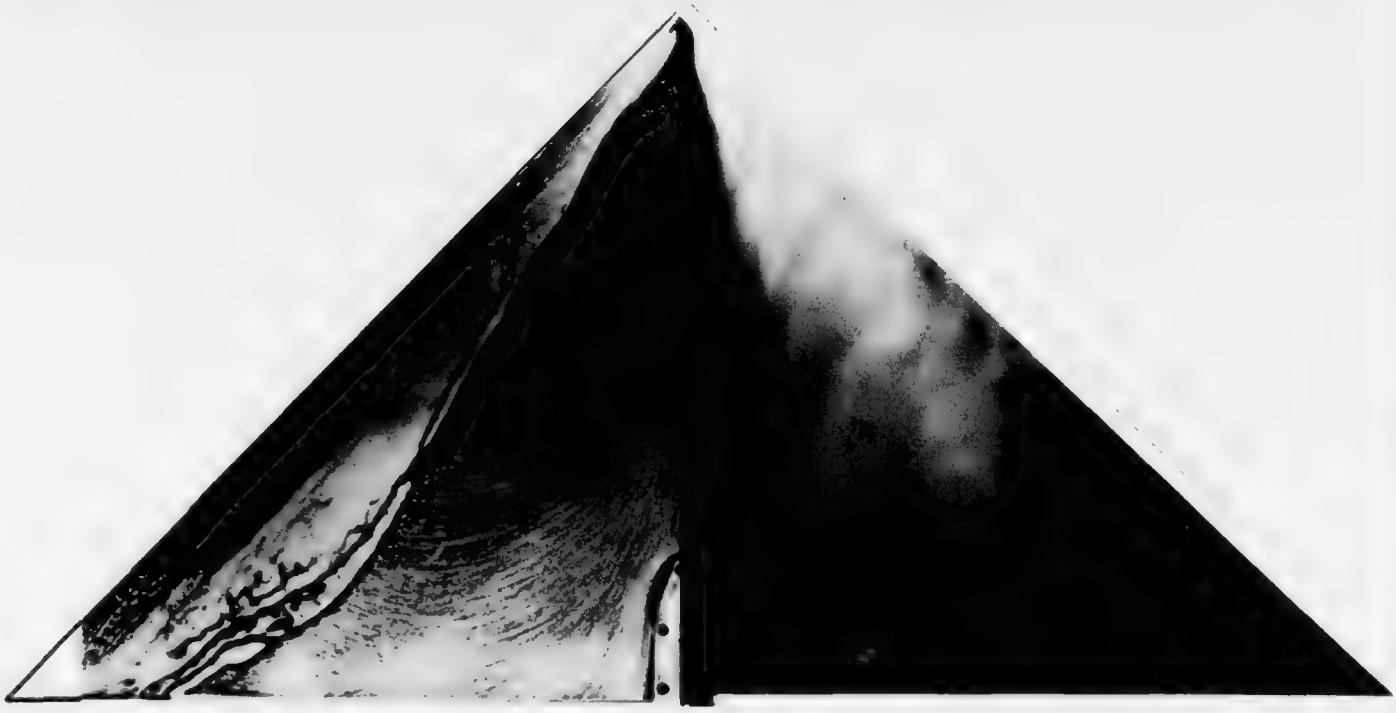

FIG. 11d $\alpha = 20°$

FIG. 11e $\alpha = 25°$

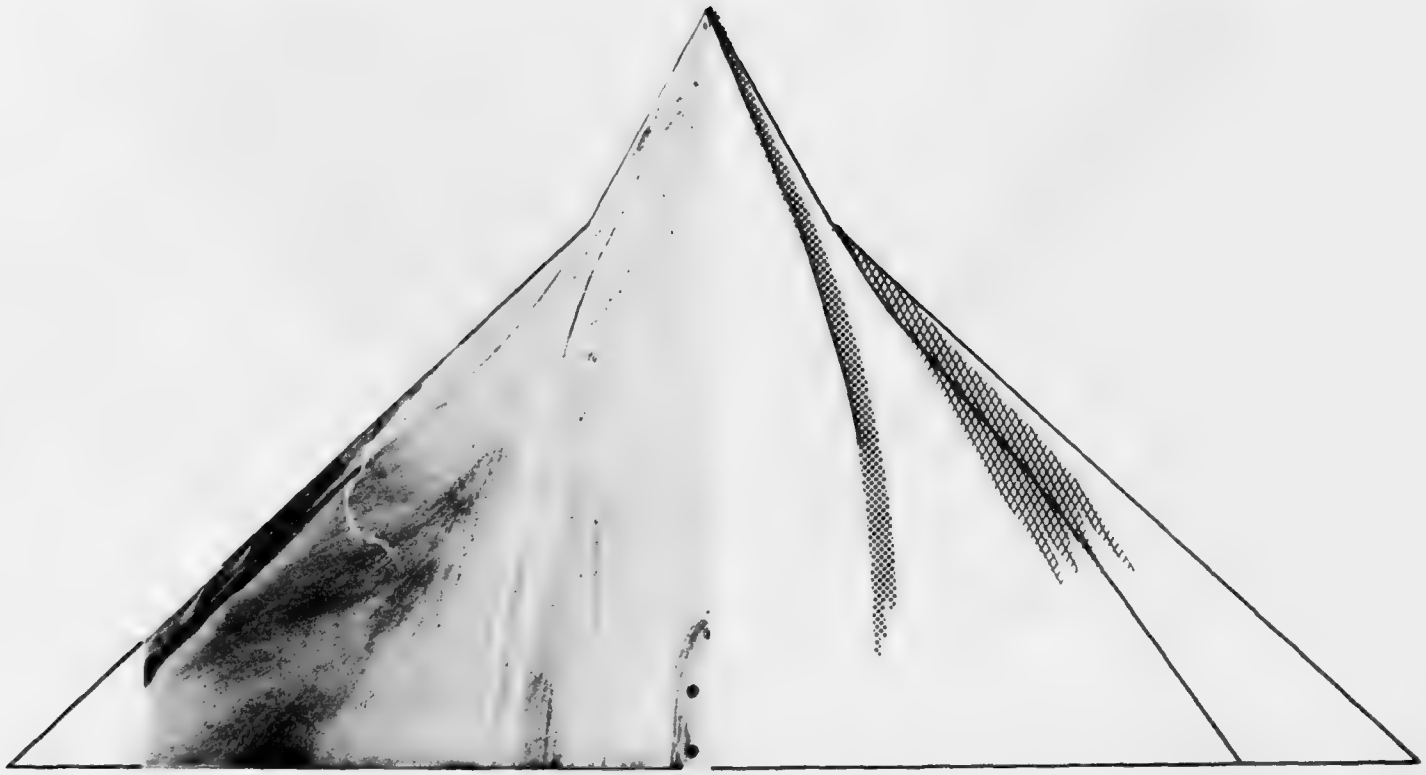

FIG. 12a SURFACE FLOW PATTERN AND VORTEX STRUCTURE OVER AR2-A2 WING, α = 5°

FIG. 12b $\alpha = 10°$

FIG. 12c $\alpha = 15°$

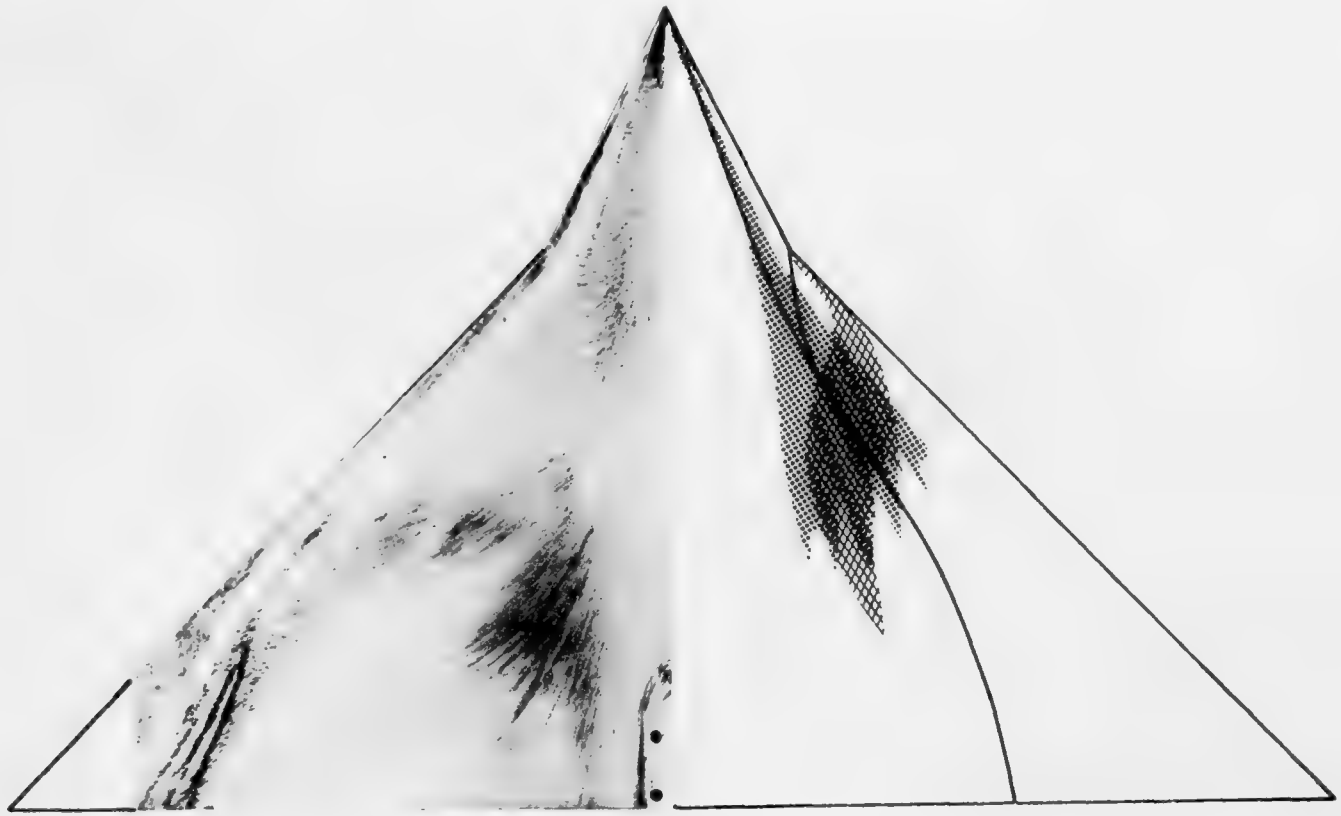

FIG. 12d $\alpha = 20°$

FIG. 12e $\alpha = 25°$

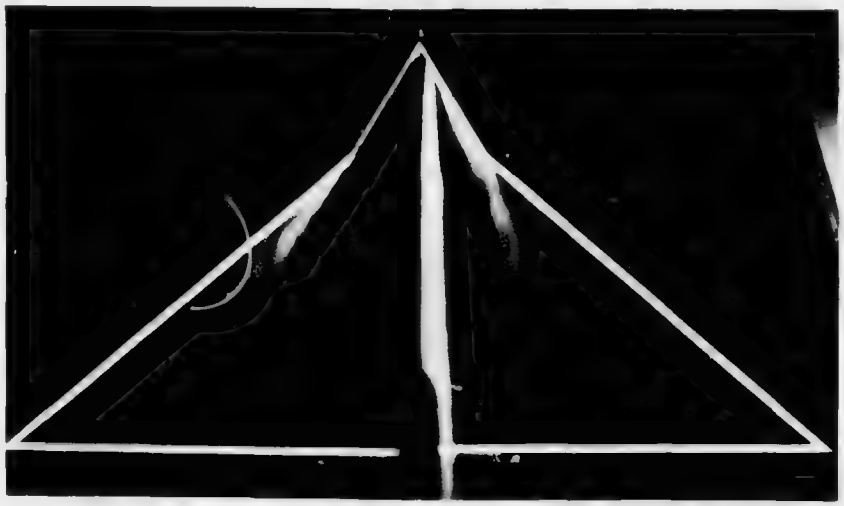

FIG. 13a VORTEX STRUCTURES OVER AR2-A2 WING, α = 5°

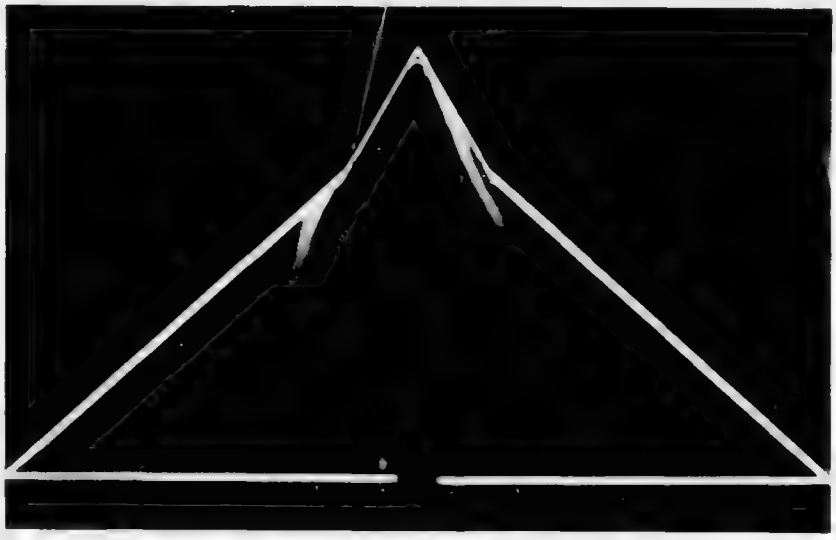

FIG. 13b α = 10°

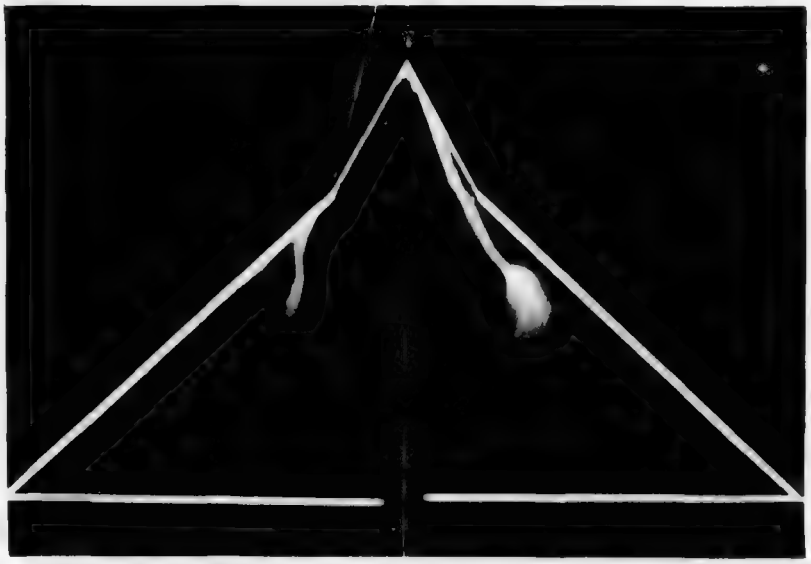

FIG. 13c $\alpha = 15°$

FIG. 13d $\alpha = 20°$

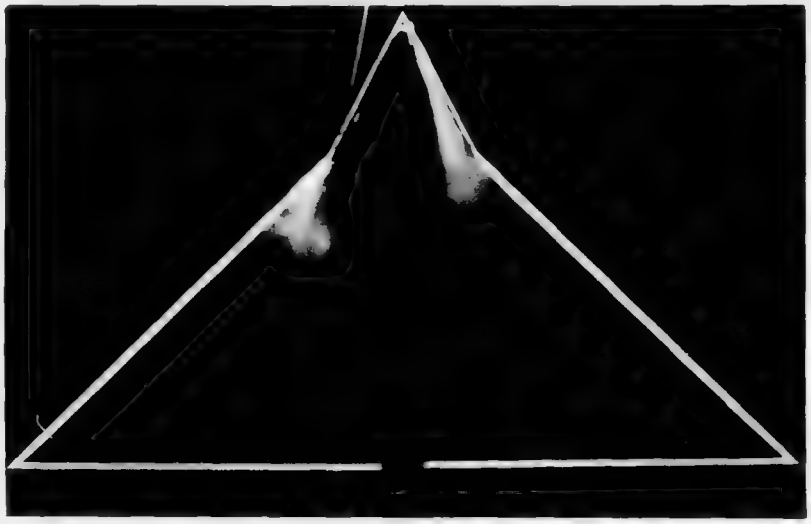

FIG. 13e $\alpha = 25°$

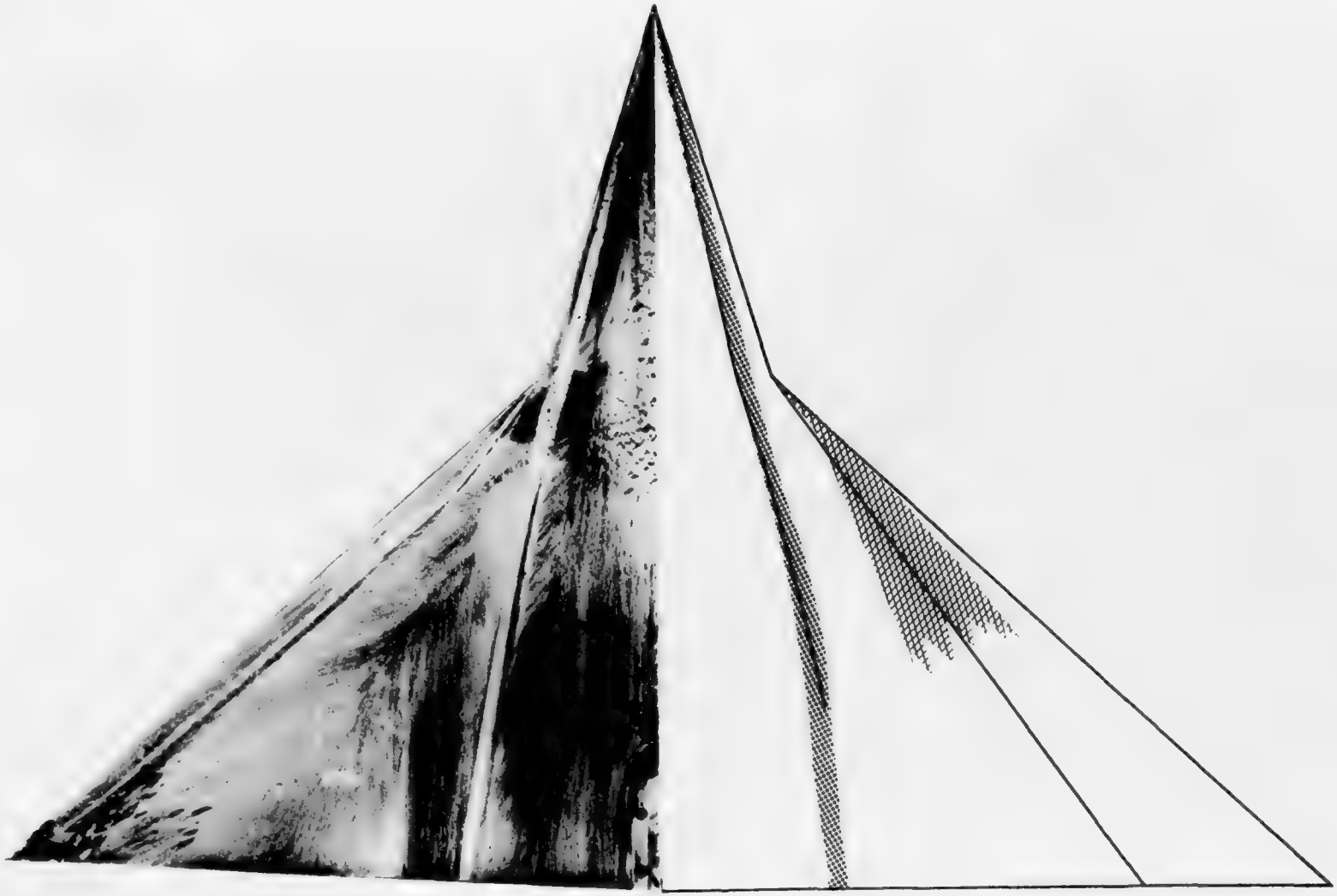

FIG. 14a SURFACE FLOW PATTERN AND LINES OF MAXIMUM SUCTION ON AR4-A1 WING, $\alpha = 5°$

FIG. 14b $\alpha = 10°$

FIG. 14c $\alpha = 15°$

FIG. 14d $\alpha = 20°$

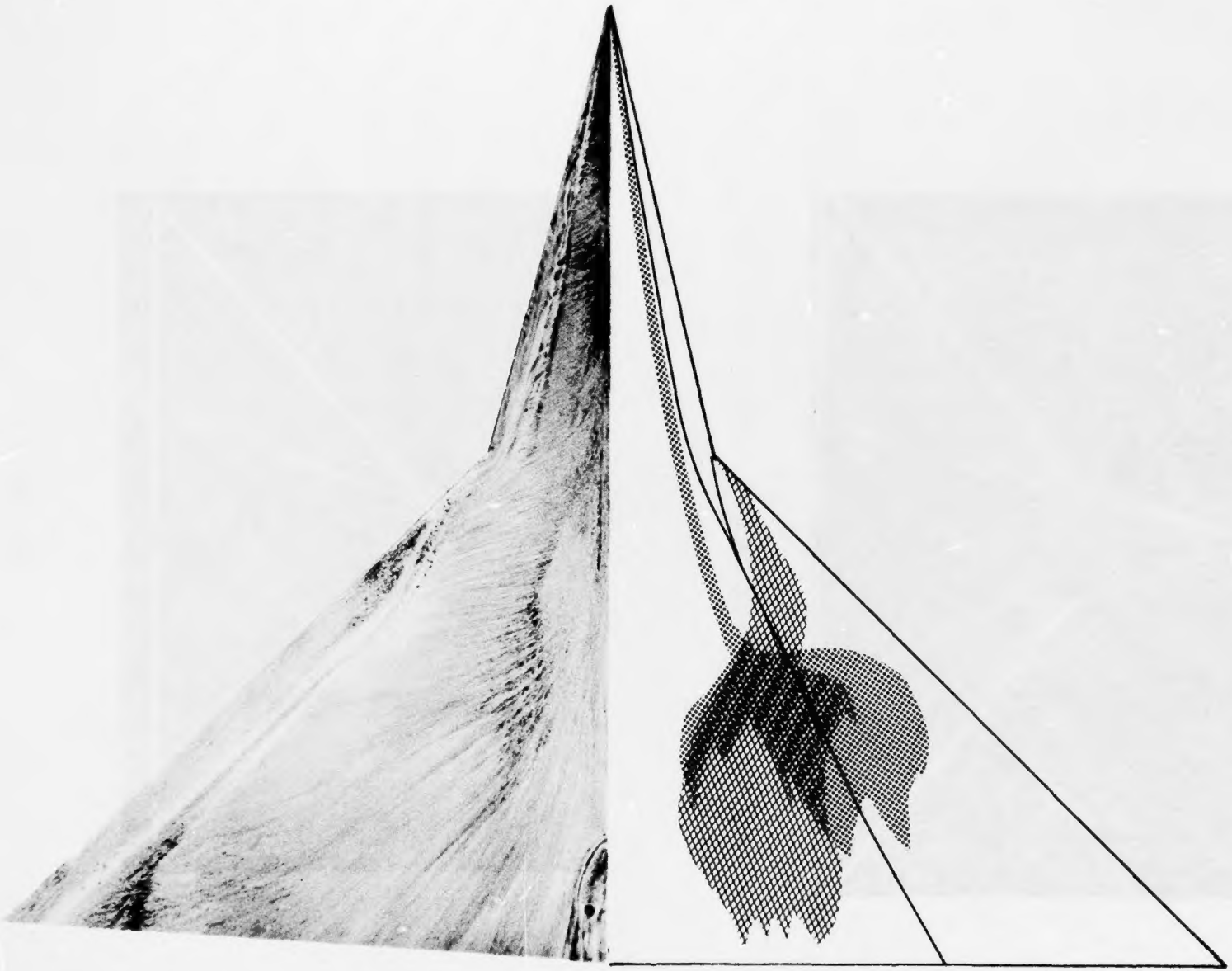

FIG. 14e $\alpha = 25°$

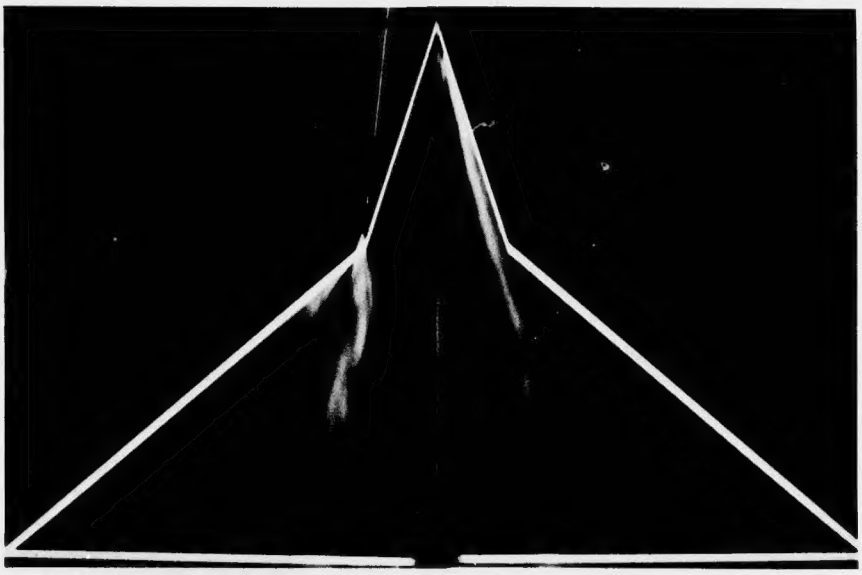

FIG. 15a VORTEX STRUCTURES OVER AR4-A1 WING, $\alpha = 5°$

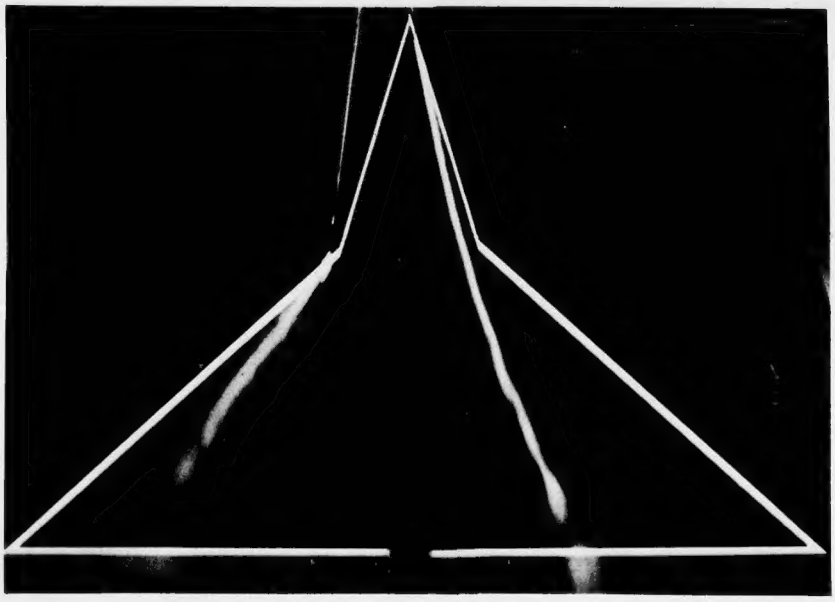

FIG. 15b $\alpha = 10°$

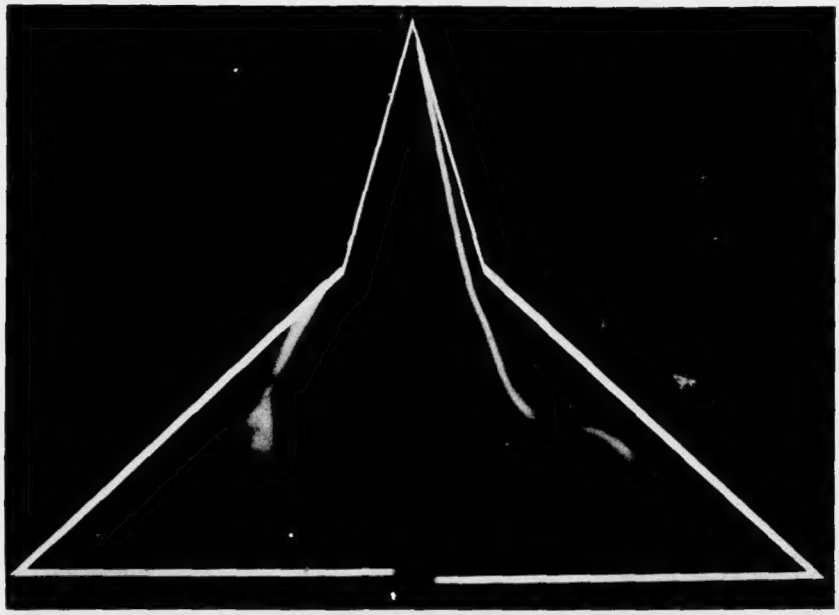

FIG. 15c $\alpha = 15°$

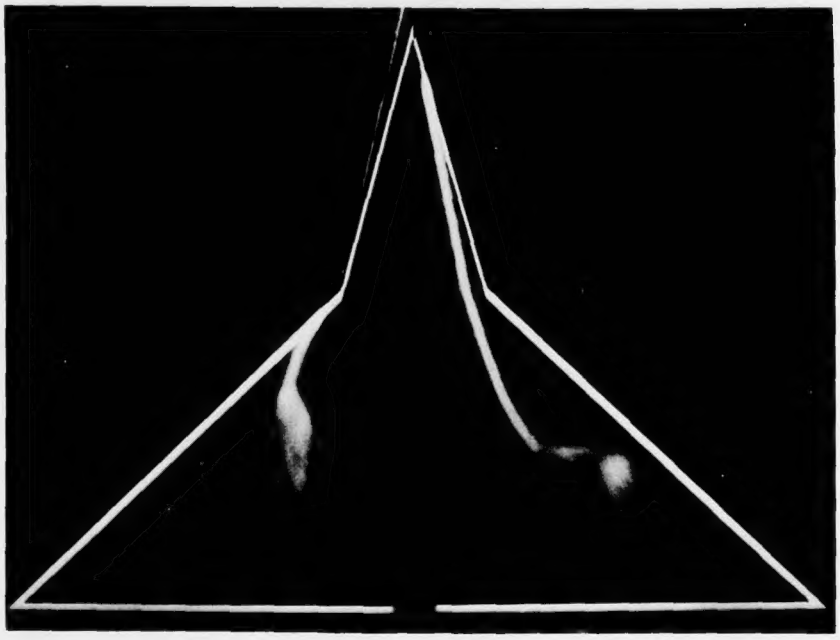

FIG. 15d $\alpha = 20°$

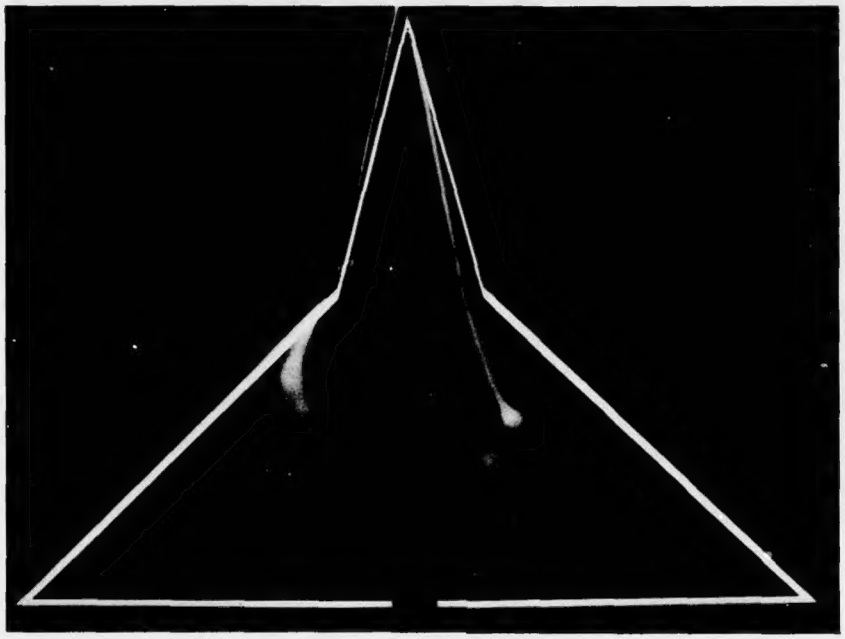

FIG. 15e $\alpha = 25°$